

K-Ar illite-mica age constraints on the formation and reactivation history of the El Doctor fault zone, central Mexico

Diana Elizabeth Garduño-Martínez^{1,*}, Teresa Pi Puig², Jesús Solé²,
Michelangelo Martini², and Jorge René Alcalá-Martínez²

¹ Posgrado en Ciencias de la Tierra, Instituto de Geología, Universidad Nacional Autónoma de México, Ciudad Universitaria, 04510 Coyoacán, México DF, Mexico.

² Instituto de Geología, Universidad Nacional Autónoma de México, Ciudad Universitaria, 04510 Coyoacán, México DF, Mexico.

* daniel_31@hotmail.com

ABSTRACT

The tectonic history of the Mexican Fold and Thrust Belt exposed in the Sierra Madre Oriental can be assessed in detail by dating the activation of the major shortening structures. The aim of this paper is to present mineralogical and K-Ar geochronologic data of illite-mica from the El Doctor thrust fault, a kilometer-scale structure exposed in the central-western Mexican Fold and Thrust Belt. Such a structure is a brittle-ductile shear zone characterized by subgreenschists facies peak conditions. The crystallization ages of neoformed clay-micaceous minerals from the core of this shear zone are used to constrain the tectonic activity along the selected shear zone. A total of 17 lutite samples were collected from different structural levels of the shear zone. The samples were characterized petrographically and detailed mineralogy was determined by X-ray diffraction. Grain-size subfractions were separated from 11 selected samples, which were subsequently used for K-Ar dating. The mesostructural and microstructural analyses, supported by K-Ar geochronologic data, permitted reconstruct of the crystallization history of phyllosilicate phases related to the tectonic activity of the shear zone. Our data indicate that the El Doctor thrust fault records a complex structural evolution, which is represented by at least three superposed deformation phases. The first phase consists of the shear zone activation, which produced a main foliation pervasive at the submillimeter-scale defined by neoformed illite-mica. This phase is constrained at 80–75 Ma, which is the range of K-Ar ages obtained by illite-mica from the coarse-grained subfractions collected at the core of the shear zone. Subsequent tectonic phases produced the reactivation of the El Doctor shear zone, which produced folding and crenulation of the previous foliation, successively cut by meter-scale extensional shear bends. The most recent reactivation phases, including diagenesis, are constrained to an age of 50–40 Ma obtained from the finest illite subfractions. Based on our data, we conclude that the El Doctor thrust fault recorded a complex, multi-phase structural evolution, characterized by a phase of activation during the Campanian period, and at least one post-Cretaceous reactivation event. The whole history of orogenic wedge construction is preserved in the El Doctor fault.

Key words: authigenic illite; dating; Sierra Madre Oriental; Laramide.

RESUMEN

La historia tectónica del Cinturón Mexicano de Pliegues y Cabalgaduras, el cual se encuentra expuesto en la Sierra Madre Oriental, puede ser reconstruida con mayor precisión mediante la datación del movimiento a lo largo de las principales estructuras de acortamiento. El objetivo de este artículo es presentar los datos mineralógicos y geocronológicos de K-Ar obtenidos para filosilicatos (illite-mica) asociados a la cabalgadura de El Doctor, una estructura de extensión kilométrica localizada en la parte centro-occidental del Cinturón Mexicano de Pliegues y Cabalgaduras. Dicha estructura es una zona de cizalla frágil-ductil, la cual alcanzó facies de subesquistos verde durante su actividad principal. Las edades de neocrystalización de minerales arcillo-micáceos en el núcleo de la zona de falla se utilizan para datar la actividad de dicha estructura. Para realizar este estudio se tomaron 17 muestras de lutita situadas a diferentes distancias del plano principal de la cabalgadura. Las muestras se caracterizaron petrográficamente y se determinó su mineralogía por Difracción de Rayos X. De 11 muestras seleccionadas, se separaron diferentes fracciones granulométricas que fueron datadas por el método K-Ar. Los análisis meso- y micro-estructural, apoyados por el análisis geocronológico de las diferentes fracciones granulométricas, permitieron reconstruir la historia de crecimiento de los filosilicatos en relación a la actividad de la zona de cizalla. Los resultados sugieren una evolución estructural compleja para la falla de El Doctor, la cual cuenta con, por lo menos, tres etapas de deformación distintas. La primera etapa es representada por la activación de la zona de cizalla de El Doctor y el desarrollo de una foliación penetrante a la escala submilimétrica con una edad de 80–75 Ma, que es el rango de las edades de illite-mica obtenidas de las subfracciones de 2–0.5 μm del núcleo de la zona de cizalla. Los sucesivos eventos de deformación consisten en la reactivación de la zona de cizalla de El Doctor y determinan el plegamiento y crenulación de la foliación anteriormente desarrollada, así como el desarrollo de zonas de cizalla extensionales a la escala métrica que cortan a los pliegues. Los eventos de reactivación más tardíos superpuestos probablemente a diagénesis están constreñidos a un rango de 50–40 Ma, edades obtenidas de la illite separada de las fracciones finas. Con base en estos datos, concluimos que la falla el Doctor presenta una evolución estructural compleja caracterizada por un episodio de activación principal en facies de subesquistos verde durante el Campaniano, seguido, por lo menos, por

un evento de reactivación postcretácico. El rango temporal completo de construcción de la cuña orogénica en esta región está preservado en la falla de El Doctor.

Palabras clave: illita autigénica; datación; Sierra Madre Oriental; Laramide.

INTRODUCTION

The occurrence of authigenic and synkinematic clay-mica minerals is a common feature in fault zones. Isotopic dating of these minerals has been used extensively in the last 20 years to assess the timing of faulting episodes and to reconstruct the tectonic evolution of mountain belts (Lyons and Snellenburg, 1971; Clauer *et al.*, 1997; Vrolijk and van der Pluijm, 1999; Zwingmann and Mancktelow, 2004; Solum *et al.*, 2005; Schleicher *et al.*, 2006; van der Pluijm *et al.*, 2006; Siebel *et al.*, 2010; Zwingmann *et al.*, 2010a, 2010b; Duvall *et al.*, 2011; Surace *et al.*, 2011; Verdel *et al.*, 2011a, 2011b; Zwingmann *et al.*, 2011; Tagami, 2012; Clauer, 2013; Viola *et al.*, 2013; Middleton *et al.*, 2014; Torgersen *et al.*, 2015). The fundamental premise of isotopic dating of faults is that the formation of fault rocks is the result of various physical and chemical processes related to fluid circulation, pressure and temperature conditions during the deformation. Therefore, the understanding of thermal regimes of fault zones, together with detailed mineralogical and textural observations, is crucial for the thermochronologic interpretation of radiometric clay-mica ages. Although K-Ar dating of illitic clay frac-

tions in fault zones has been used by many authors, the interpretation of these data is sometimes difficult because the different mechanisms of illite growth in faults are controversial (e.g. Srodoń, 2002). The Mesozoic and Cenozoic geologic history of Mexico is characterized by an abundant record of orogenic events, but isotopic dating of fault related clay-mica minerals was only sparsely applied (e.g. Gray *et al.*, 2001; Fitz-Díaz *et al.*, 2014). This led to an incomplete reconstruction and understanding of the structural evolution of Mexico, which is the key to interpreting the tectonic history of North America.

In this paper, we present a combination of structural, petrographic, mineralogical and K-Ar isotopic data from the El Doctor thrust fault, which is considered a major structure of the Late Cretaceous-Paleogene Laramide orogen in Mexico (Suter, 1984, 1987). These data represent the first contribution to clay-mica dating of faults obtained at the Laboratories of the Instituto de Geología (Universidad Nacional Autónoma de México), and serve as a starting point for the development of such methodologies in Mexico. The results obtained will be integrated with previous data and will be interpreted in the framework of the Laramide orogenic evolution proposed by previous authors.

GEOLOGICAL SETTING

The Mexican Fold and Thrust Belt (MFTB) is a remarkable morphotectonic feature in the geology of Mexico because of its extent and prominent topographic expression in the Sierra Madre Oriental (Figure 1). This belt is interpreted as a dominantly thin-skinned

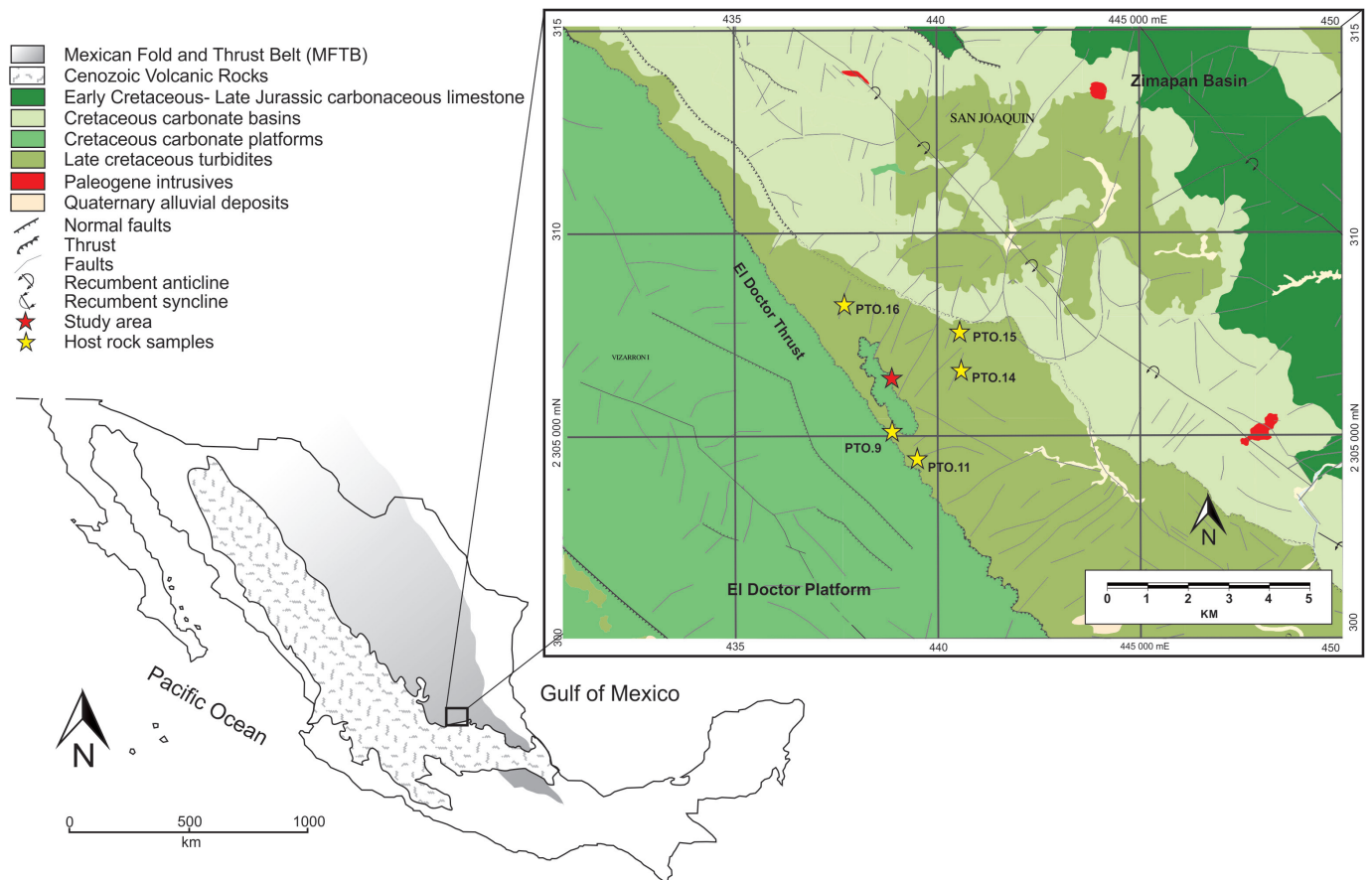


Figure 1. Schematic geological map showing the location of the study area, the extension of the Mexican Fold and Thrust Belt (MFTB) and the Cenozoic volcanic rocks. Modified from Martini *et al.* (2012).

Late Cretaceous-Early Paleogene orogenic wedge that formed by considerable horizontal shortening of the continental interior of Mexico (Suter, 1984, 1987; Fitz-Díaz, 2010; Fitz-Díaz *et al.*, 2011). In the Peña de Bernal-Tamazunchale area, the MFTB displays an eastward-tapering wedge shape and a gradient in the deformation and temperature progressively decreasing to the east (Fitz-Díaz *et al.*, 2011). According to the orogenic wedge models of Dahlen *et al.* (1984) and Dahlen (1990), these characteristics indicate that the “bulldozer” producing such a regional deformation should have been located to the west of the MFTB, and that shortening must have propagated progressively to the east. This is supported by paleontologic data, which indicates that the synorogenic deposits across the Peña de Bernal-Tamazunchale section are progressively younger to the east (López-Ramos, 1983; Hernández-Jáuregui, 1997).

At least, two different shortening phases have been documented in the MFTB (Fitz-Díaz *et al.*, 2012). D1 is considered as the main tectonic event that built up the Sierra Madre Oriental and is expressed by kilometer-scale, T1 thrusts and F1 folds that accommodated several hundred kilometers of shortening (Suter, 1980, 1984, 1987; Ortega-Flores, 2010; Fitz-Díaz *et al.*, 2012). Based on stratigraphic constraints, this deformation event took place between the Turonian and Santonian periods in the western MFTB, and between the Campanian and Maastrichtian periods in its eastern part (Hernández-Jáuregui, 1997). D2 is expressed only by gentle F2 folds and meter-scale displacements on late T2 thrust faults superposed to D1 structures (Ortega-Flores, 2010; Fitz-Díaz *et al.*, 2012). F2 folds and T2 faults affected Late-Cretaceous deposits, which provide a temporal limit to this second deformation event (Fitz-Díaz *et al.*, 2014). D1 and D2 are interpreted by Fitz-Díaz *et al.* (2011) as the result of the Sevier and Laramide orogenies, respectively. According to this scenario, the MFTB is the product of a complex Late Cretaceous-Early Paleogene structural evolution which resulted from the superposition of at least two different orogenic pulses. Finally, the MFTB is cut by high-angle post Eocene normal and oblique faults that produced a complex horst and graben structural pattern. The El Doctor thrust fault is exposed in the western part of the Peña de Bernal-Tamazunchale section (Figure 1). This structure was described as a northeast-southwest (NE-SW) trending, moderately SW dipping, brittle-ductile T1 shear zone which produced the top-to-the-NE overriding of Aptian-Albian platform limestones

of the El Doctor Formation onto Turonian-Lower Santonian (Omaña Pulido, 2012) calcareous turbidites of the Soyatal Formation, which were interpreted as the syntectonic deposits related to the D1 orogenic event (Suter, 1987). Considering that this shear zone is a major structure representative for the evolution of western MFTB, we took an exposure of the El Doctor thrust to test the potential of illite-mica in dating low-intermediate grade faults, as well as for improving the reconstruction of the Late Cretaceous-Early Paleogene structural evolution in central Mexico. The outcrop selected for this study is located to the west of Querétaro, Mexico (Figure 1).

METHODOLOGY

Sampling and sample preparation

Structural data of the fault zone and surrounding outcrops were collected during the fieldwork. These comprise fault, foliation and axial plane surfaces, fold axes, and lineations. Oriented samples were collected and cut parallel to the XZ plane of the finite strain ellipsoid, in order to determine the kinematics of the main structures and the mineral phases which compose the foliation surfaces.

A total of 17 unweathered lutite samples of 200–500 g were collected for clay characterization from a 30 m long traverse across the Soyatal Formation, which is exposed in the footwall of the El Doctor thrust fault (Figures 1 and 2). The hanging wall of the fault was not sampled because lutite strata are practically absent in the El Doctor Formation. Eight samples were collected from the core of the main fault zone, which is designated in this work as Zone 1. This zone extends from the tectonic contact between the El Doctor and Soyatal Formations to ~5 m depth into the footwall. Nine samples are from less pervasively deformed rocks of the outer part of the fault zone, which is designated in this work as Zone 2. This zone is ~25 m thick and extends downward from the lower boundary of Zone 1 to the last strata displaying clear evidence of deformation related to the T1 El Doctor thrust fault. Four host rock samples (Figure 1) were also collected to determine their mineralogy and to ascertain the presence of detrital or diagenetic illite and mica.

Samples were prepared following standard X-ray diffraction (XRD) procedures (Moore and Reynolds, 1997) and the recommendations by the IGCP 294 IC working group (Kisch, 1990). Sample sizes of

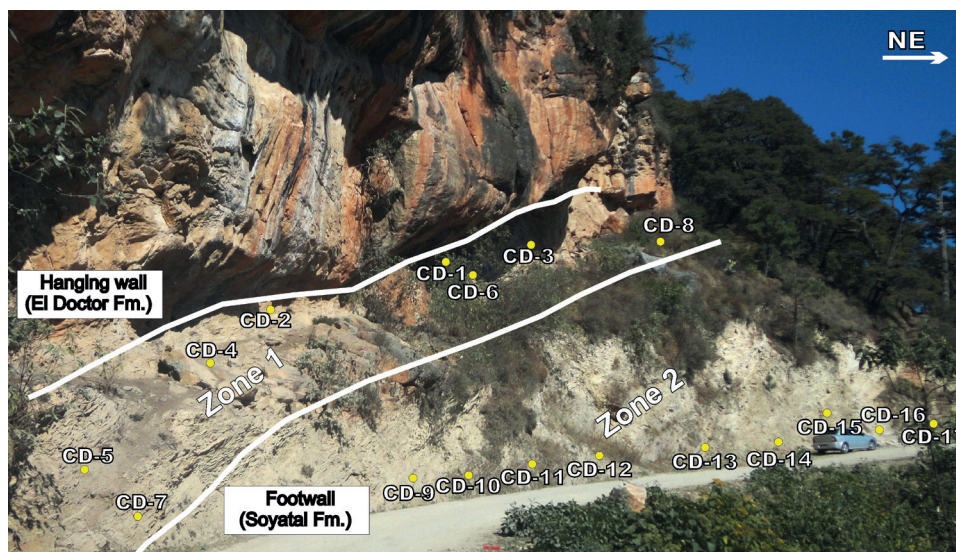


Figure 2. Photograph of the sampling site at the El Doctor fault, showing sample locations.

50–100 g for each lutite sample were used for clay separation. Samples were gently disaggregated to avoid artificial grain size reduction of rock components (Liewig *et al.*, 1987). Each sample was broken into small chips (2 mm) using a porcelain crusher and subsequently dispersed in deionized water. For clay separation, we used the most unaggressive method (Jackson, 1985; Moore and Reynolds, 1997). Grain size fractions of <2 μm and 2–4 μm were separated in distilled water according to Stoke's law. A portion of the <2 μm fraction obtained by sedimentation was centrifuged in order to extract the coarse (2–0.5 μm), medium (0.5–0.05 μm) and fine (<0.05 μm) clay fractions. Coarse-grained fractions (2–4 μm) were investigated in three samples from the fault and four samples from the host rock, far away from the fault, to evaluate the influence of potential contamination from detrital or diagenetic protolith minerals.

From the <2 μm fractions, air-dried oriented preparations were obtained by pipetting some drops of the Mg-saturated suspensions onto a glass slide, which was then dried at 30 °C for a few hours (Moore and Reynolds, 1997). Ethyleneglycol solvation of the slides was achieved by exposing them to ethyleneglycol vapor at 70 °C for a minimum of 12 hours. Randomly oriented samples were prepared by packing 150–250 mg of dried material as small clay spheres which were cut and mounted in low background sample holders.

X-ray diffraction

The mineralogy of the different size fractions was determined by XRD. Measurements were made using a Shimadzu XRD-6000 diffractometer at the Instituto de Geología, of the Universidad Nacional Autónoma de México (UNAM), operating with an accelerating voltage of 40 kV and a filament current of 30 mA, using CuK α radiation and a graphite monochromator. Non-oriented samples from each whole rock were measured over a 2θ angular range of 4–70 ° at a speed of 1 °(2 θ)-min⁻¹.

Oriented clay samples were examined by XRD in the air-dried form, after saturation with ethyleneglycol and after heating at 450 °C and 550 °C. All preparations were measured over a 2θ range of 4–70 ° (air-dried) and 4–40 ° (glycolated and heated) at a speed of 1 °(2 θ)-min⁻¹. Glycolated XRD analyses were carried out to investigate potential occurrence of expandable mixed layer smectite minerals (Moore and Reynolds, 1997). Identification and analysis of clay minerals by XRD has been described by Brindley and Brown (1980) and Moore and Reynolds (1997).

The Kübler index (KI), a measure of illite 'crystallinity', was measured using the full width at half maximum (FWHM) of the 10 Å illite peak on oriented clay preparations from the <2 μm fraction (Kübler, 1967, 1968; Kübler and Jaboyedoff, 2000) and expressing the results in terms of the Bragg angle 2θ . We use the term 'illite-mica' when it is not possible to distinguish between the two minerals by XRD (KI near 0.25) and includes illite and clay-sized muscovite.

Identification of illite and evaluation of the percentage of expandable layers in mixed illite/smectite were made using the methods described by Środoń (1984), Środoń and Eberl (1984), Reynolds (1992) and Moore and Reynolds (1997).

Illite polytype quantification was made by comparison between the diffractograms for randomly oriented samples of different fractions and simulated patterns calculated using WILDFIRE software (Reynolds 1993, 1994), adjusting the effects of preferred orientation. The WILDFIRE patterns are calculated considering a mixture of 1M polytype (60 % cv, $P_0=1$ and $P_{60}=0$) with 2M1 polytype (Drits *et al.*, 1995; Drits *et al.*, 1998) in different proportions. Polytype quantification was calculated only for the coarse and total fractions of samples dated by K-Ar. There was not enough material available from smaller fractions to run the appropriate measurements.

For polytype identification, intensities were recorded at 0.04 ° 2θ step intervals from 10 to 40 °, using 40 seconds counting time per step. Sizes of the divergence slit, anti-scatter and receiving slits were 1°, 1°, and 0.15 mm, respectively.

The percentage of 2M1 illite-mica relative to 1M illite was determined from the ratio $I(2.80\text{Å})/I(2.58\text{Å})$ (Maxwell and Hower, 1967) for all samples, and by comparison of high-resolution patterns from randomly oriented samples with calculated patterns using the WILDFIRE software (*e.g.*, Grathoff and Moore, 1996; Ylagan *et al.*, 2000, 2002).

Semi-quantification of clays by X-ray diffraction

The proportion of clay species was estimated semi-quantitatively from oriented preparations using simple peak weighting factors. For area estimation we used the Fityk software for nonlinear curve fitting (Wojdyr, 2010). The glycolated XRD trace was separated into illite, smectite and mixed-layer peak areas by calculation of the percentage of these areas (Moore and Reynolds, 1997; Środoń *et al.*, 2001).

Peak decomposition

A mathematical decomposition procedure has been systematically applied to air-dried patterns in the 6 ° to 13 ° 2θ region (Lanson and Besson, 1992; Lanson, 1997) using the Fityk peak fitting software (Wojdyr, 2010). The first step of the procedure was the subtraction of the background from the pattern. The second step was the calculation of curves which fit the experimental diffractogram using the least-squares method. We used two curves for the decomposition of the air-dried samples. The 10.1–10.5 Å peak (Gaussian curve) is the 001 reflection of a poorly crystallized illite (PCI). The sharper peak (Gaussian curve), closer to 10 Å, corresponds to particles having a large crystallite size such as mica or a well crystallized illite (WCI).

Electron microscopy

Some samples have been imaged by scanning electron microscopy (SEM) to observe the actual morphology of mica and illite. Freshly broken rock surfaces of rock chips were cleaned in an ultrasonic bath, gold coated and examined in mixed secondary and backscattered electron mode using the MEB Nova-2000 NANOLAB scanning electron microscope at the Instituto Mexicano del Petróleo. The SEM was operated at 30 kV and a current less than 20 nA, and equipped with an energy dispersive X-ray analyzer (EDS-Genesis 4000). In general, illite clusters are characterized by a dense meshwork of platy clay minerals and a minor proportion of fine-grained authigenic fibrous clay material.

K-Ar dating

Dating of clay fractions was performed using the K-Ar dating method. The methodology used is a modification of the classical technique, specifically designed to date small amounts of sample. For potassium (K) analysis we use X-ray fluorescence with high dilution fused pearls to minimize both the amount of sample (50–100 mg) and the matrix effects (Solé and Enrique, 2001). For argon (Ar) quantification, a CO₂ laser system is used for sample fusion, followed by gas cleaning and measurement in a MM1200B noble gas mass spectrometer at Instituto de Geología, UNAM. This technique is able to measure samples in the milligram range and is described in detail by Solé (2009).

RESULTS

Structural and petrographic observations

The detailed structural analysis of the El Doctor fault zone allows the identification of at least four superposed groups of structures, which we identify as D1 to D4. The D1 group is represented by the

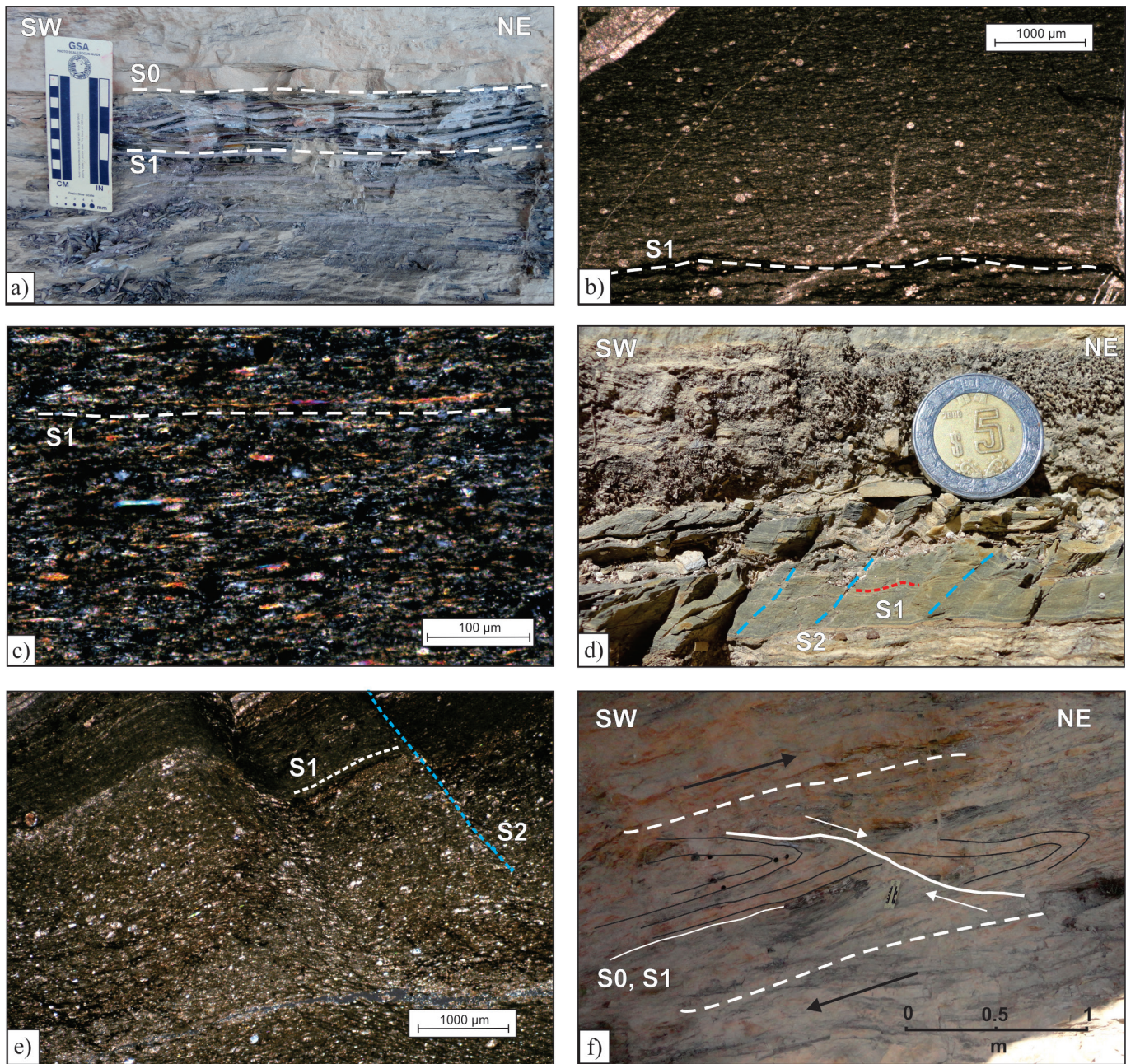


Figure 3. (a) S1 foliation parallel to the S0 bedding planes, S1 is pervasive at the submillimeter-scale. (b) Smooth to anastomosing foliation defined by oxides; main deformation mechanism: pressure solution (calcite). (c) S1 foliation defined by fine-grained phyllosilicates; main deformation mechanism: pressure solution and crystallization (phyllosilicates). (d) and (e) S2 foliation is pervasive at the submillimeter-scale, S2 is a spaced crenulation cleavage superposed on S1, and defined only by fine-grained seams of opaque minerals. (f) F2 folds are cut by meter-scale, NW-SE striking, NE gently dipping extensional shear (green line).

El Doctor thrust fault, a brittle-ductile shear zone which produced the overriding of Aptian-Albian platform limestone of the El Doctor Formation onto the Turonian-Santonian synorogenic turbidites of the Soyatal Formation. Such a T1 shear zone is associated with a NW-SE striking, SW dipping S1 foliation parallel to the S0 bedding planes (Figure 3a). S1 is pervasive at the submillimeter scale in Zone 1, which is the core of the shear zone, and progressively becomes less penetrative at the shear zone boundaries. In lutites of the Soyatal Formation, S1 is a slate cleavage defined by aligned phyllosilicates, fine-grained slaty minerals and oxides (Figures 3b and 3c). Phyllosilicate content decreases progressively from the core to the boundary of

the shear zone, suggesting the occurrence of a temperature gradient normal to the fault surface. In sandstones of the Soyatal Formation, S1 varies from a spaced, disjunctive, smooth foliation to anastomosing foliation. Cleavage domains consist primarily of fine-grained seams of opaque minerals, whereas microlithon domains are composed of recrystallized calcite and scarce low- to moderately-elongated quartz grains with pressure shadows, undulose extinction, and locally subgrain domains. In platform limestone of the El Doctor Formation, S1 is a spaced, smooth to stylolitic foliation defined by fine-grained opaque minerals. Such microtextural evidence suggests that S1 was formed mostly by pressure-solution processes and minor crystal-

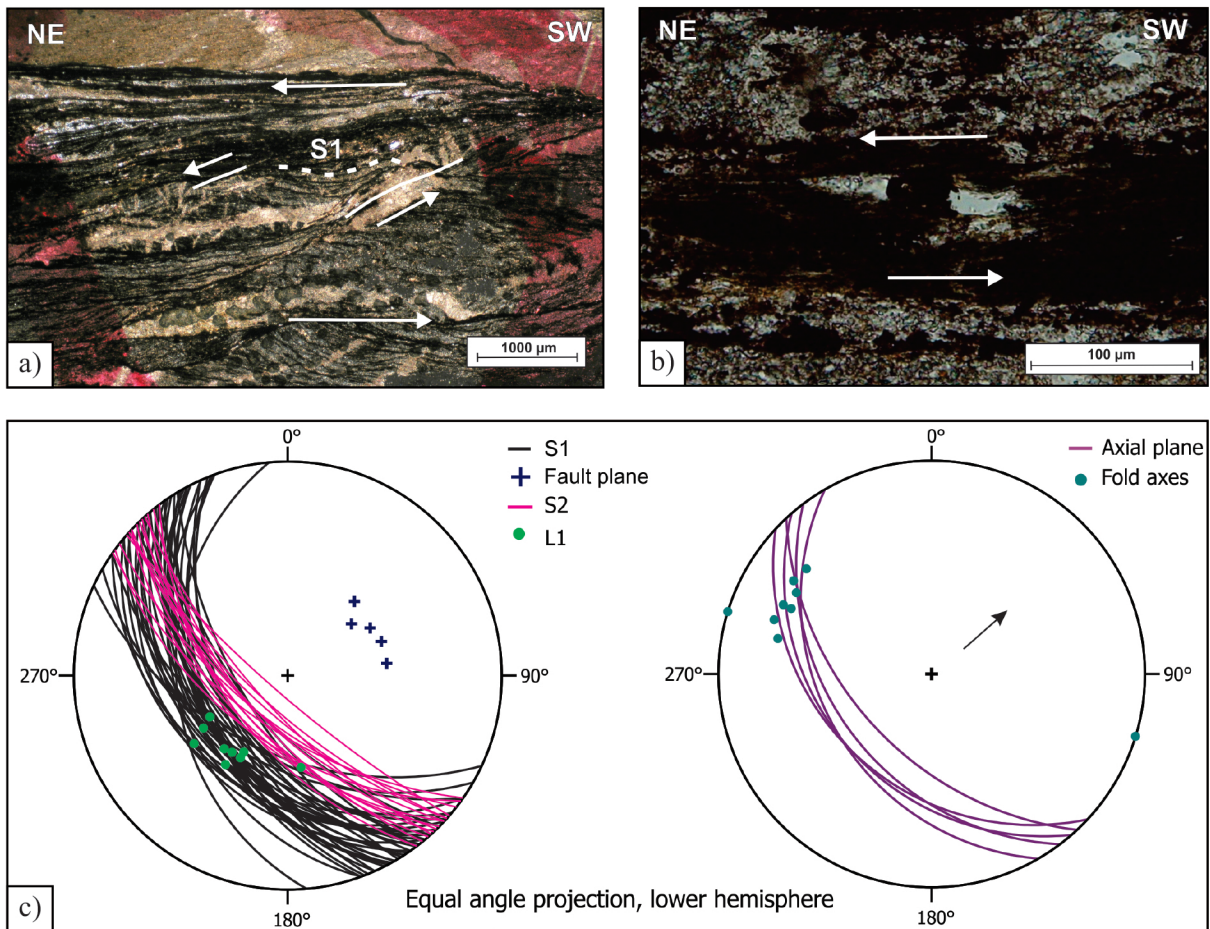


Figure 4. (a) S-C' microstructures observed on cuts parallel to the XZ-plane of the finite strain ellipsoid. (b) Asymmetric porphyroclasts observed on cuts parallel to the XZ-plane of the finite strain ellipsoid indicate a top-to-the-NE tectonic transport for the El Doctor thrust. (c) Equal angle, lower hemisphere projections of great circles to S1, S2 and poles to L1 thrust-related lineations. Fold axes and axial plane are also plotted in the stereographic nets, showing a top-to-the-NE tectonic transport.

plastic deformation, which indicates that structures of the D1 group were formed at temperatures $<400\text{ }^{\circ}\text{C}$ (e.g. Passchier and Trouw, 1998). This is also supported by the syntectonic crystallization of phyllosilicates and slaty minerals, which suggests a low greenschists or subgreenschists metamorphic grade. Scarce S-C microstructures and asymmetric porphyroclasts observed on cuts parallel to the XZ-plane of the finite strain ellipsoid indicate a top-to-the-NE tectonic transport for the El Doctor thrust (Figures 4a and 4b), which is in agreement with the kinematics reported by previous authors.

Structures of the D2 group are represented by meter-scale, NE-overturning, tight F2 folds that developed exclusively in the Soyatal Formation, either in Zone 1 or in Zone 2. The F2 folds display NW-SE striking, NW gently plunging axis, and are associated with an S2 axial plane foliation which is evident only in lutite layers. S2 is a spaced crenulation cleavage superposed on S1, and is defined only by fine-grained seams of opaque minerals (Figures 3d and 3e).

The F2 folds are cut by meter-scale, NW-SE striking, gently NE dipping extensional shear bends that were observed exclusively in the Zone 1 turbidites from the Soyatal Formation (Figure 3f).

Finally, high-angle normal faults cut pre-existing D1-3 structures and are associated with centimeter to decimeter-thick gouge and cataclasis.

Whole-rock mineralogy

All analyzed samples were collected from the Soyatal Formation, since it is the only unit containing shale strata at the study outcrop.

The whole-rock mineralogy comprises quartz, calcite, minor plagioclase, feldspar, illite-mica, smectite, kaolinite, vermiculite and traces of chlorite, which are present in variable proportions. XRD analyses of all the samples are summarized in Table 1.

The host rock mineralogy is not uniform and all outcrops show evidences of deformation. The four analyzed samples confirm the presence of quartz, calcite, minor plagioclase and phyllosilicates in the whole-rock (Figure 5). Using separated clay fractions from host rocks, illite-mica (KI <0.25 in coarse fractions), kaolinite and chlorite were identified in variable proportions. Minor smectite or vermiculite was also detected by XRD.

Mineralogy of clay subfractions

All subfractions display a clay assemblage consisting of illite-mica with scarce kaolinite in Zone 1, changing into an illite-mica, smectite, vermiculite and traces of chlorite paragenesis in Zone 2 (Table 2). Illite-mica is the major clay mineral component and the unique K-bearing phase of all clay subfractions.

Pure smectite and mixed-layer minerals were identified only in the coarse and medium fractions, respectively, of four samples from

Table 1. Whole rock mineralogy.

Sample	Distance to shear plane (m)	Coordinates	Phy	Qz	Cc	H	G	Pg
<i>Zone 1</i>								
D1	0.05			Thin section				
CD1	0.1		x	xx	x	o		o
Doc1	0.25	Thin section						
CD2	0.25		x	xx	o	o	o	o
CD3	0.7	14Q 0438716	x	xx	x	o		o
CD4	1.0	2306465	x	xx	xx			o
CD5	1.2		x	xx	xx			o
CD6	1.22		o	xx	xx			
CD7	1.7		x	xx	o			o
CD8	2.7		x	xx	x	o		o
<i>Zone 2</i>								
CD9	13.85		x	xx	o			o
CD10	15.25		x	xx	xx	o		o
D14'	15.55		Thin section					
CD11	16.6		x	xx	xx			o
CD12	16.65		x	xx	x			o
CD13	20.0	14Q 0438716	x	xx	xx			o
CD14	21.4	2306465	x	xx	x			o
D11'	21.4	Thin section						
D10	22.95	Thin section						
CD15	24.3		xx	xx	o			o
CD16	26.46		x	xx	xx			o
CD17	29.16		x	xx	xx			o
<i>Host rock (Soyatal Fm.)</i>								
PTO. 9		14Q 0438609 2305129	x	xx	xx			x
PTO. 11		14Q 0439484 2304551	o	xx	xx			o
PTO. 14		14Q 0440549 2306716	o	xx	xx			o
PTO. 15		14Q 0440802 2307702	o	xx	xx			o
PTO. 16		14Q 0437639 2308573	x	xx	xx			o

Phy: phyllosilicates. Qz: quartz. Cc: calcite. H: hematite. G: goethite. Pg: plagioclase. xx: >25%. x: 10-25%. o: <10%.

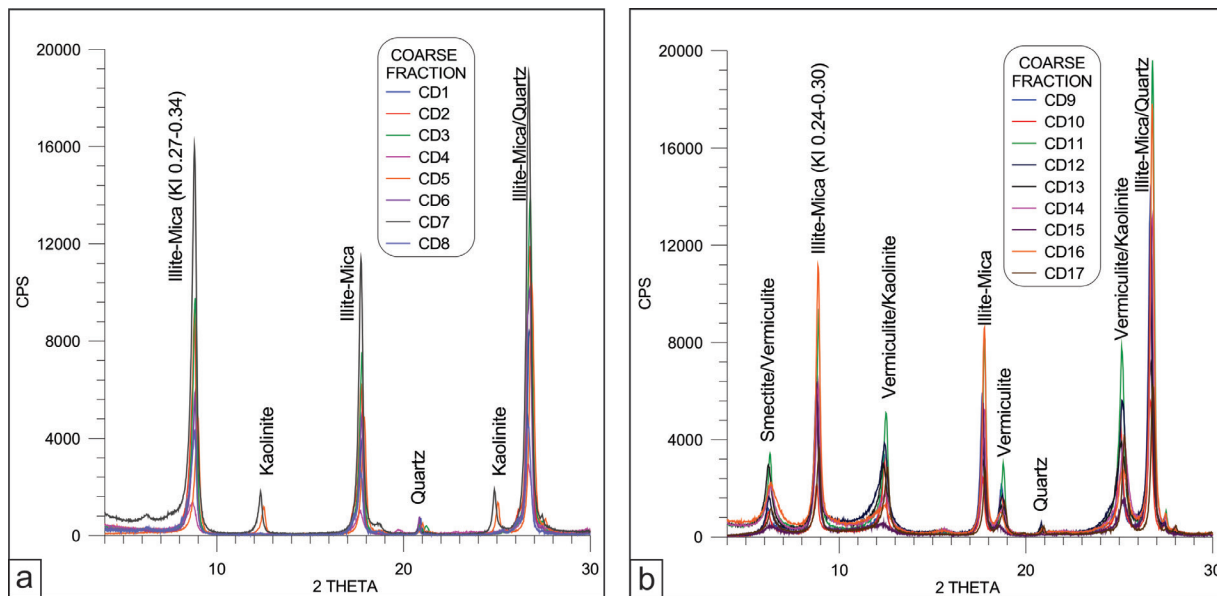


Figure 5. Representative X-ray diffractograms of <2 μm clay fractions from the El Doctor fault. (a) Zone 1: consists mainly of illite-mica with some kaolinite. (b) Zone 2: consists mainly of mica-illite, smectite and vermiculite.

Table 2. Clay fraction mineralogy.

Sample	Size	Qz	G	Cc	Pg	Chl	K	V	Sm	I/S	I/M	CS	KI	Zone#	%2M1*	%2M1	%WCI	%PCI	KI (WCI)	KI (PCI)	
<i>Zone 1</i>																					
CD1	VC	xx		o							xx	103	0.25	E					0.17	0.48	
	T	x									xxx	67.2	0.33	A	33.7	40	51	49	0.24	0.51	
	C	x									xxx	77.3	0.30	A	62.5	50	55	45	0.36	0.61	
	M			o								xxx	36.8	0.52	D	30.8	40	53	47	0.28	0.64
	F		x									xxx	17.2	1.0	D					0.6	1.15
CD2	T	x									xxx	67.2	0.33	A	15.8	45	41	59	0.22	0.56	
	C	x									xxx	81.3	0.29	A	22.4	50	35	65	0.17	0.43	
	M			o							xxx	39.6	0.49	D	59.1	40	55	45	0.33	0.67	
CD3	VC	xx		o							xx	118.9	0.23	E					0.18	0.51	
	T	o									xxx	85.8	0.28	A			50	50	0.24	0.49	
	C	x									xxx	90.9	0.27	A-E	40.2	55	60	40	0.23	0.41	
	M			o							xxx	46.8	0.43	D	23.3	45	54	46	0.31	0.58	
CD4	T	x									xxx	70.2	0.32	A			40	60	0.23	0.46	
	C	xx									xx	70.2	0.32	A			46	54	0.35	0.58	
	M	x									xxx	36.8	0.52	D			44	56	0.21	0.51	
CD5	T	x					x				xxx	77.3	0.30	A			54	46	0.24	0.48	
	C	x					x				xxx	85.8	0.28	A			46	54	0.22	0.44	
	M			o			o				xxx	46.8	0.43	A			49	51	0.31	0.59	
CD6	T	x		o							xxx	77.3	0.30	A			49	51	0.23	0.51	
	C	x		o							xxx	77.3	0.30	A			59	41	0.22	0.42	
	M			o	o						xxx	55.2	0.38	A			59	41	0.33	0.58	
CD7	T	x					x	o			xxx	81.3	0.29	A			38	62	0.21	0.43	
	C	x					x	o			xxx	90.9	0.27	A-E			46	54	0.24	0.47	
	M			o			o	x			xxx	40.7	0.48	D			57	43	0.39	0.78	
CD8	VC	xx		o							x	257.5	0.16	E					0.16	0.44	
	T	x				o					xxx	55.2	0.38	A			35	65	0.24	0.55	
	C	x				o					xxx	64.4	0.34	A	39.0	50	38	62	0.23	0.51	
	M			o					o	xxx	31.5	0.59	D	15.9	40	52	48	0.42	0.69		
<i>Zone 1</i>																					
CD9	T	x	o			x	x		x		xx	96.6	0.26	A-E	16.3	55	57	43	0.22	0.62	
	C	o				x	x		o		xx	96.6	0.26	A-E	59.0	50	55	45	0.24	0.7	
	M			o		o				xxx	x	32.2	0.58	D	14.8	40	56	44	0.46	0.73	
CD10	T	x						x	x		x	90.9	0.27	A-E			41	59	0.21	0.49	
	C	x						x	x		xx	81.3	0.29	A			45	55	0.2	0.47	
	M			o				o		xxx	x	31.5	0.59	D			67	33	0.36	0.72	
CD11	T	o						x	x		xx	103	0.25	E			50	50	0.2	0.45	
	C	o						x	x		xxx	110	0.24	E			51	49	0.19	0.43	
	M			o				x		xx	x	59.4	0.36	A			28	72	0.31	0.59	
CD12	T	x						x			xx	90.9	0.27	A-E			40	60	0.21	0.53	
	C	o						x	x		xx	85.8	0.28	A			66	34	0.21	0.53	
	M			o				x		x	xx	45.4	0.44	D			42	58	0.29	0.61	
CD13	T	x						xx			x	96.6	0.26	A			39	61	0.24	0.49	
	C	x						x			xx	77.3	0.30	A			43	57	0.21	0.48	
	M			o				x		xxx	51.5	0.40	A			38	62	0.31	0.64		
CD14	T	x						x			xx	77.3	0.30	A			56	44	0.22	0.86	
	C	o						x			xx	90.9	0.27	A-E			52	48	0.22	0.51	
	M			o				x			xx	57.2	0.37	A			57	43	0.31	0.63	
CD15	T							x		xxx	96.6	0.26	A-E	29.5	60	50	50	0.23	0.5		
	C	o						x		xxx	96.6	0.26	A-E	78.2	65	57	43	0.21	0.47		
CD16	T							xx			xx	85.8	0.28	A			53	47	0.25	0.62	
	C							x		xxx	96.6	0.26	A-E			55	45	0.21	0.49		
CD17	T	x		o				x			xx	103	0.25	E			54	46	0.23	0.61	
	C	x		o				x			xx	90.9	0.27	A-E	52.0	70	54	46	0.22	0.54	

continues

Table 2 (cont.). Clay fraction mineralogy.

Sample	Size	Qz	G	Cc	Pg	Chl	K	V	Sm	I/S	I/M	CS	KI	Zone#	%2M1*	%2M1	%WCI	%PCI	KI (WCI)	KI (PCI)
<i>Host rock</i>																				
PTO.9	VC	xx		o	o		x	o			x		0.16	E						
	C	x		o	o		x	x			xx		0.24	E						
	M	o					x	x	o		xx		0.32	A						
PTO.11	VC	xx				o	o	o			x		0.18	E						
	C	x				o	x	x			xx		0.28	A						
	M					o	x	x			xx		0.34	A						
PTO.14	VC	xx		x		o	x				x	309	0.15	E					0.1	0.3
	C	x		o	o	x	x				xxx	110.4	0.24	E						
	M	x				o	x		o		xxx	59.4	0.36	A						
PTO.15	VC	xx				o	o	x			x	220.7	0.17	E					0.13	0.44
	C	x				o	o	x			xxx	128.8	0.22	E						
	M					x	xx				xx	85.8	0.28	A						
PTO.16	VC	xx		o	o		x	x			x	220.7	0.17	E					0.14	0.5
	C	x				o	x	x			xx	110.4	0.24	E						
	M					o	x	x	o		xx	70.2	0.32	A						

xxx = >65 %, xx = 65–45 %, x = 45–10 %, o = <10 %. T: <2 µm total fraction. VC: very coarse (4–2 µm). C: coarse fraction (2–0.5 µm). M: medium fraction (0.5–0.05 µm). F: fine fraction (< 0.05 µm). Qz: quartz. Cc: calcite. Pg: plagioclase. Chl: chlorite. K: kaolinite. V: vermiculite. Sm: smectite. I/S: illite/smectite. I/M: illite-mica. CS: crystallite size. KI: Kübler Index. WCI: well crystallized illite. PCI: poorly crystallized illite. #: Metamorphic grade. D: Diagenesis. A: Anchizone. E: Epizone. %2M1*: illite polytype quantifications using the equation $[I(2.80 \text{ \AA}) / I(2.58 \text{ \AA})]$. %2M1: illite polytype quantifications using WILDFIRE.

Zone 2. Considering the subgreenschist metamorphic grade of the shear zone we infer that smectite minerals postdate the main fault movement.

Illite Kübler index (KI) and crystallite size (CS) were calculated (shown in Table 2) and used for the evaluation of the kinematic history of phyllosilicate-bearing rocks assuming anchizone limits of $0.25^\circ 2\theta$ and $0.42^\circ 2\theta$ KI index (Kübler, 1968; Kisch, 1991).

Illite from Zone 1 samples contains more than 95% of illite-mica in all coarse fractions. This suggests illite crystallization at temperatures higher than 250 °C (Abad, 2006), which is in good agreement with the temperature inferred for the subgreenschist metamorphic grade of the El Doctor shear zone. The individual KI values measured for samples from Zone 1 range from 0.26 for the coarse fractions to 0.58 for the medium fractions. Converted to the Kübler scale, these define a temperature range which varies from the epizone-anchizone limit to the diagenetic field (Kübler, 1968; Kisch, 1991). Crystallite size (CS) is between 32 and 97 nm for the medium and coarse fractions, respectively, of Zone 1. SEM images (Figure 6) reveal that illite crystallites in Zone 1 have a strong preferred orientation and exhibit platy morphologies, which suggest *in situ* neocrystallization. In synthesis, the detailed sample characterization presented in this work supports the authigenic origin of illite-mica for samples from Zone 1.

The KI values for different size fractions of Zone 2 range from 0.24 to 0.59, whereas the CS is between 31 and 110 nm for the medium and coarse fractions, respectively. KI values for <2 µm illite in Zone 2 are similar to the values obtained for Zone 1. Only for >2 µm fractions of Zone 2, the KI values are smaller than in Zone 1, which suggests the influence of detrital phases in these >2 µm fractions. The presence of smectite and vermiculite is interpreted as late low-temperature transformation.

Clay polytype characterization

For the studied samples, the amount of 2M1 ranges from 40–55%

in both Zone 1 and Zone 2, except for three samples of Zone 2 which have 60 to 70%. This variation is related to size fraction, and all the finest fractions are richer in 1M polytype than the coarsest fractions. The high-temperature authigenic illite (2M1) from the El Doctor shear zone cannot be distinguished from detrital muscovite (2M1). Considering the presence of illite-mica foliation ($T > 300^\circ \text{C}$; Passchier and Trouw, 1998) we interpret that detrital mica might be present only in the very coarse fractions (>2 µm). In this sense, the quantification of illite polytypes cannot be used to measure the relative proportions of detrital and authigenic illite from the El Doctor shear zone.

Decomposition of the illite 001 XRD peak (Figure 7a) from oriented preparations also indicates mixtures of two illites (Meunier and Velde, 2004; Meunier *et al.*, 2004). The differentiation and quantification between poor crystallized illite (PCI) and well crystallized illite (WCI) is a convenient way to describe the illite population. The presence of PCI influences the global peak position (shift towards lower angle) and peak FWHM (peak broadening). The relative abundance of the PCI peak is expressed as a percentage. Decomposed peak positions are expressed in Å, whereas FWHM are expressed in 2θ CuK α (Table 2). The percentage of PCI accounts for the relative proportion of illite crystallites with lower crystallite size.

Proportions of WCI range from 35 to 67%. In general, high abundances of WCI are associated with the coarse fractions and low abundances are associated with the finest fractions. Peak decomposition values give similar percentages of WCI to those derived from the analysis of the random powder data using the WILDFIRE software (Table 2) for 2M1. The peak widths of PCI and WCI diminish together (Figure 7b), indicating that there is a simultaneous growth of both components in different size fractions.

K-Ar data

We dated 31 clay fractions from 12 samples, seven from the fault zone and five from the host rock. K-Ar analyses of <0.5 to 4 µm frac-

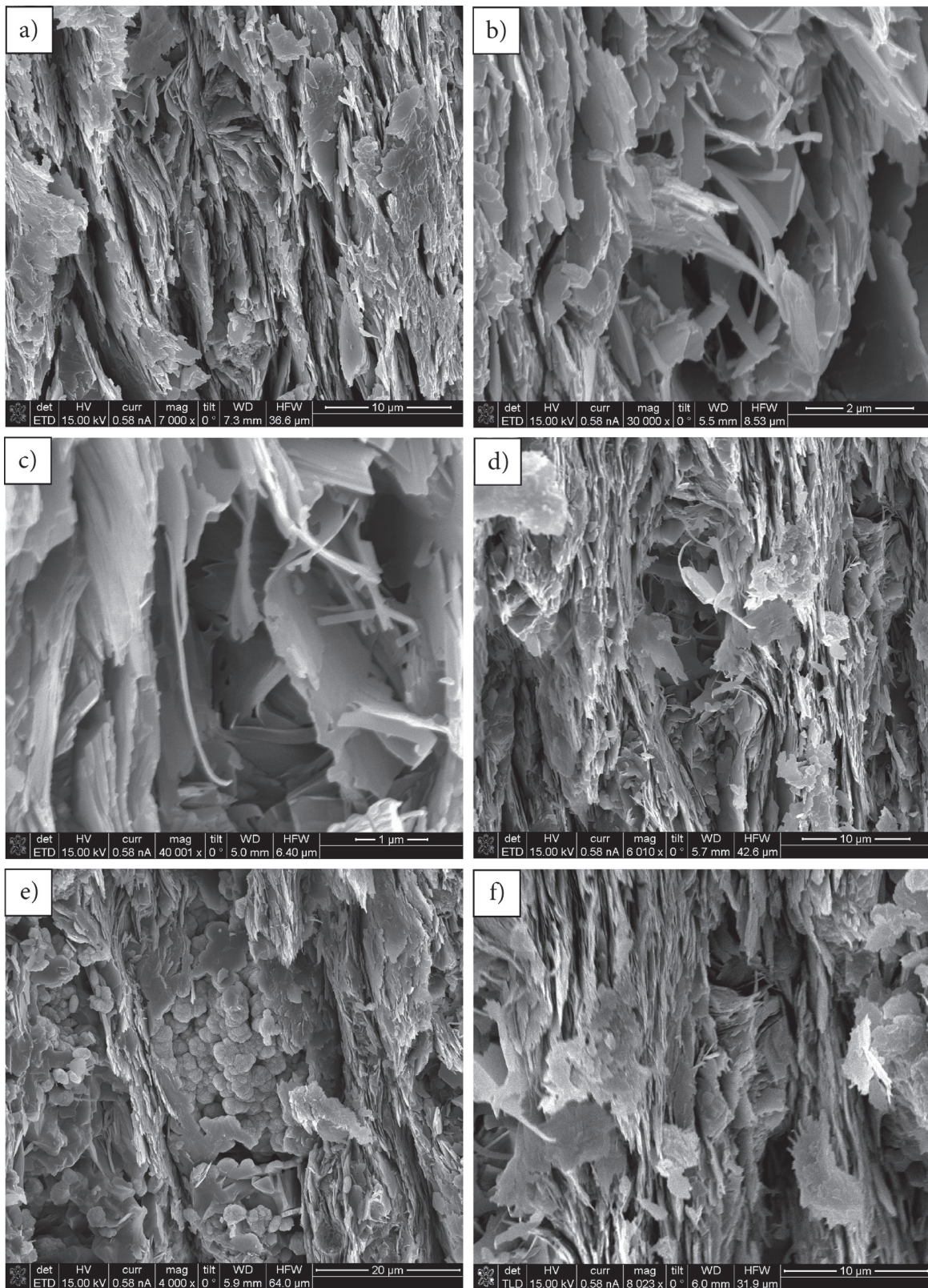


Figure 6. Electron microscopy (SEM) images of illite from the El Doctor fault. Image (a) illustrates the typical sample surface within, a 10 µm overview, made of coarse authigenic illite with predominantly platy habit from sample CD1. The size of the authigenic minerals can be related to the lower greenschist facies reached during the main deformation and crystallization event. Note that the coarse illite flakes delineate the foliation, an indication of authigenic origin. Illite mineral species was confirmed by EDS analysis. Images (b), (c) and (d) illustrate authigenic filamentous and lath illite from the finest fraction, which represents the last illite grown in the fault rock. Authigenic illite fibers growth from platy particles [(d) and (f)] and can extend up to several µm. In image (e), the sub-µm rosettes growing on the illite are secondary iron oxides (hematite). SEM image evidences the growing of these crystals by processes of dissolution-precipitation associated with faulting.

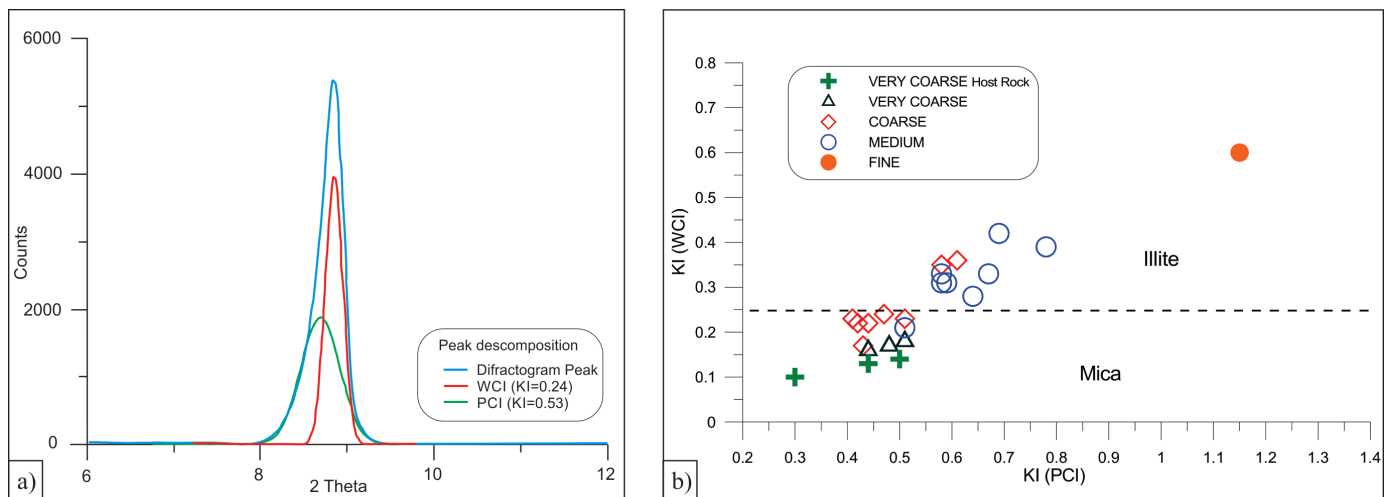


Figure 7. (a) Example of illite 001 peak decomposition using the Fityk 0.9.3 software (Wojdyr, 2010). (b) Correlation of KI of WCI and KI of PCI for different clay fractions. WCI = well crystallized illite, PCI = poorly crystallized illite.

tions separated from different samples yielded ages ranging from 97.9 ± 1.6 Ma to 39.1 ± 0.8 Ma (1σ) (Figure 8 and Table 3). Radiogenic ^{40}Ar ranges from 88 to 99% indicating small to very small atmospheric contamination. All $<2 \mu\text{m}$ clay fractions from the fault zone are younger than the Lower Santonian (86 Ma), the paleontological age of the upper part of the Soyatal Formation (Omaña Pulido, 2012).

K-Ar ages become younger with increasing KI and the smaller size fractions are the youngest. The K-Ar ages for the fault zone (CD samples) from very coarse (4–2 μm) illite fractions range between 90 and 81 Ma (70 Ma for the CD8 sample that has been affected by a later shear bend, Figure 3f). For coarse (2–0.5 μm) illite fractions the K-Ar ages range between 80 and 72 Ma. For medium (0.5–0.05 μm) and fine grained ($<0.05 \mu\text{m}$) illite fractions, the K-Ar ages range between 71 Ma and 66 Ma, and 50 Ma, respectively. Ages from the host rock (PTO samples) show a range of 98 to 80 Ma for the very coarse (2–4 μm) illite fraction, a range of 84 to 72 Ma for the coarse (2–0.5 μm) illite fraction, a range of 67 to 59 Ma for the medium (0.5–0.05 μm) illite fraction, and an age of 40 Ma for a $<0.05 \mu\text{m}$ fraction. The host rock display ages that are equal or older than the stratigraphic age of the Soyatal Formation for the 4–2 μm fractions and smaller fractions show higher age dispersion than the samples from the fault (Figure 8).

DISCUSSION

Dating of diagenesis and faults

The use of the K-Ar dating of clay minerals to decipher the history of a sedimentary rock is an old methodology dating back to the first decade of the K-Ar technique (Hurley *et al.*, 1959). It has been quickly recognized that K-Ar ages of such samples do not give the correct age of the sediment. The ages were either too old or too young. Bailey *et al.* (1962) measured for the first time the polytypes 2M1 and 1Md using the K-Ar method on samples from the Pennsylvanian shale. The 2M1 polytype was much older than the stratigraphic age, and the 1Md was much younger. From these pioneering works up to the present, considerable effort has been made in the interpretation of the K-Ar age of clay minerals, mainly illite.

The dating of tectonic processes using clays is even more complex. Not having, in most cases, alternative approaches to the K-Ar or Ar-Ar methods (and Rb-Sr in some cases), we must date grain-size fractions

of some samples taken from both the fault zone and the host rock, the latter far away from the influence of the fault. The basic reason for doing so is that the development of authigenic clays in a fault zone is a convolution of two processes: recrystallization and growth *due to burial* (diagenesis s.s.) and recrystallization and growth *due to strain* (tectonics s.s.). Complete deconvolution of the two processes is difficult. If the ages are older than the minimum stratigraphic age, then illite is mainly detrital and no more information can be obtained (except for provenance studies). If the ages are younger than the stratigraphic age, three cases can be envisaged: (1) illite is neoformed, (2) illite has lost a fraction of its initial argon, or (3) illite is a mixture of both neoformed and detrital types.

The interpretation of geochronological data from faults has been somewhat controversial, due to the complexity of the problem caused mainly, but not exclusively, by the small grain size of clay minerals that impedes true mechanical separation of the different phases (*e.g.* detrital illite, authigenic illite). Thus, the actual interpretation of data is dependent on the methodology used. Systematic attempts to date fault movement by the use of K-Ar or Ar-Ar geochronometers date from the 1990s (*e.g.* Hamilton *et al.*, 1992; Clauer and Chaudhuri, 1995) but was accentuated after the work of van der Pluijm *et al.* (2001). Two schools of thought emerged, one based on the use of the classical K-Ar method, and other on the use of the Ar-Ar method. The latter was championed by the publication of the 2M1-1M illite age analysis (Hunziker *et al.*, 1986; Pevear, 1999) and the ‘retention age’ approach (Dong *et al.*, 1995). In the last few years the controversy was accentuated by the finding that the illite age approach was not useful in many cases (*e.g.* Zwingmann *et al.*, 2010a) and also because the ‘retention age’ interpretation has been discredited by one of the authors who proposed the original idea (Middleton *et al.*, 2014). Some K-Ar versus Ar-Ar age arguments have also been published (Clauer, 2013) with no clear conclusion for either methodology. Torgersen *et al.* (2015) made a detailed study of a fault in Norway and proposed a conceptual model which is a synthesis of previous ideas applied to reactivated faults. In our opinion the model lacks the convolution of diagenesis described above, but is a good starting point to interpret complex faults.

Closure temperature of illite

The closure temperature (Dodson, 1973) of illite for the K-Ar geochronometer has never been determined experimentally. Nevertheless,

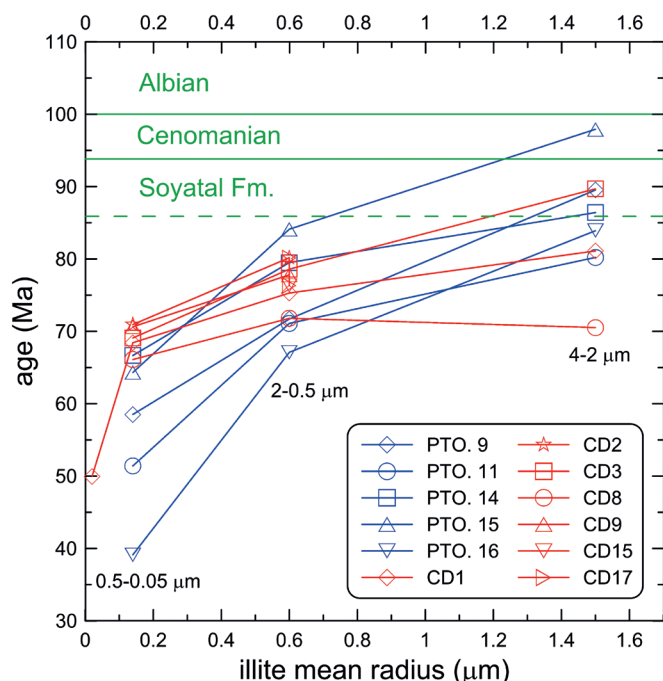


Figure 8. Summary of K-Ar ages plotted against mean radius of illite fractions from the study area. CD samples are from the fault zone and PTO samples are from the Soyatal Formation far from the El Doctor fault. The stratigraphic age of the Soyatal Formation is also displayed. CD8 has been sampled on a later shear, showing the youngest age from very coarse fractions. The significance of this age (~70 Ma) is uncertain, but can represent the true age of the movement of the secondary fault (see text).

an approximate number is necessary for data interpretation. To solve this unknown, two different values can be used: (1) the empirical temperature of 260 °C for the argon closure of an illite of ~2 μm grain size (Hunziker *et al.*, 1986); or (2) the use of muscovite diffusion parameters (Harrison *et al.*, 2009). In Table 4 we show the closure temperature calculated for muscovite of different grain sizes and we can see that the closure temperature for muscovite of relevant grain size is ~300 °C. This value represents the maximum closure temperature of illite, because the muscovite structure is the most stable member of the series smectite–illite–muscovite. In other words, experimental and empirical data suggests a closure temperature lower than ~300 °C for a clay-size illite.

Temperature of the El Doctor fault and regional rocks

As discussed before, the temperature of the fault zone can be indirectly derived from the observed microstructure. The presence of foliation formed up by illite-mica (Figures 4, 6a) indicates a temperature of formation higher than 300 °C (Passchier and Trouw, 1998), in the structural zone shown in Figure 9. Regional host rocks from the El Soyatal Formation are also affected by some tectonic deformation even at several kilometers from the fault, so it is difficult (or even impossible) to find undeformed host rocks. This implies that the overall tectonic pile has been affected by the orogeny, an important point which is discussed later. In any case, the temperature at the fault zone was high enough to reset the K-Ar system of detrital micas, if present, of 2 μm of diameter or smaller, *i.e.* the clay fraction of the rock.

There is very little data about the regional temperatures reached by the Soyatal or other adjacent formations. The temperatures reported by Gray *et al.* (2001) in secondary fluid inclusions in microfractures in

the footwall rocks of El Doctor fault thrust (Figure 1), range between 245 and 250 °C and are considered as a thermal anomaly centered at the frontal edge of the fold belt near the El Doctor fault zone. This temperature window is critical for illite-mica Ar loss (*e.g.*, Merriman and Peacor, 1999) and because it is based on only a few analyses it may be interpreted as a minimum range for the burial temperature, to be related to the ‘Laramide’ orogeny (Gray *et al.*, 2001).

Mineralogy from the El Doctor fault zone and the Soyatal host rock

To interpret the results one important condition must be fulfilled; that illite-mica is the only K-bearing phase in the system. This condition has been asserted by X-ray diffraction: no other K-bearing phases were present in the <4 μm fractions analyzed. In the case of the El Doctor fault zone the hanging wall is a carbonate from the El Doctor Formation and the footwall is the detrital Soyatal Formation. Due to the monomineralic nature of the carbonate, the samples used for K-Ar dating have been taken exclusively from the Soyatal Formation. One group was taken from the fault zone and another from the host rock (Figure 1 and Table 1). The large amount of phyllosilicates in the fault, when compared to the host rocks far from the fault, indicates synkinematic mineral growth, as deduced already by the petrographic and XRD studies.

XRD data illustrates that the micas from the fault zone have a relatively large range of KI, from 0.24 to 0.59, for the different illite fractions. The WCI and PCI peaks, obtained by decomposition of each illite fraction (Table 2), give a range of KI from 0.17 to 0.46 and from 0.41 to 0.86, respectively. In the PCI versus WCI plot (Figure 7) we can see that both parameters are correlated, which is an indication of simultaneous growth (Meunier and Velde, 2004). Texturally (shown in Figure 6) we can see that fibrous illite (1M) grows after platy illite (2M1), probably by dissolution. This fact is significant because no diagenetic or metamorphic process able to form a WCI from PCI must have occurred after the main fault phase because all illite-mica would have been WCI. In other words, all PCI observed today has been formed after WCI in subsequent secondary orogenic movements or diagenesis.

Because the formation of WCI is more dependent on time than on temperature, geological processes which do not have enough time or temperature to convert all neoformed illite to the WCI component, will develop an important proportion of PCI. The dynamic process of illite formation in shales (Soyatal Formation), is governed by dissolution-recrystallization of older minerals. The original radiogenic argon is lost from detrital micas (< 2 μm) which recrystallized. The growth of neoformed illite-mica during prograde metamorphism associated with faulting most likely occurs at the expenses of pre-existing detrital mica grains following the process of dissolution/precipitation (*e.g.*, Inoue *et al.*, 1988; Jaboyedoff and Cosca, 1999). In the El Doctor fault, this process is evidenced in the petrographic study. After the main fault event, a retrogression of the neoformed illite-mica minerals occurred, with the consequent generation of 1M illite (Figure 6). Analysis of shapes and crystal size distribution (Eberl *et al.*, 1999) is important to interpret the growing process during illitization. Hairy illites are formed in short periods of time and perfect platy hexagonal crystals grow slowly. Platy subhedral habits and a strong preferred orientation demonstrate an authigenic origin.

K-Ar ages of all analyzed fractions

K-Ar ages (Table 3) are plotted in Figure 9. All data obtained from the <2 μm fractions at the fault are younger than the Middle Turonian-Lower Santonian age of the Soyatal Formation (Omaña Pulido, 2012), *i.e.* 94–86 Ma (ICS, 2014). This is a confirmation that detrital mica age has been reset during the heating of host rocks by frictional fault

Table 3. K–Ar ages from illite fractions from the El Doctor fault (CD samples) and the Soyatal Formation (PTO samples).

Sample	fraction (µm)	%K	⁴⁰ Ar* (mol/g) x10 ⁻¹⁰	%Ar*	Age (Ma)	±1σ
CD1	4–2	3.75	5.395	97.5	81.1	1.2
	< 2*	5.89	7.785	81.2	74.7	1.4
	2–0.5	6.32	8.427	97.6	75.3	1.0
	0.5–0.05	6.22	7.523	97.5	68.4	0.9
	<0.05	3.64	3.197	88.7	49.9	0.9
CD2	< 2*	6.38	9.137	98.2	80.8	1.0
	2–0.5	6.42	9.128	99.0	80.2	1.0
	0.5–0.05	6.61	8.293	99.0	70.9	1.0
CD3	4–2	4.68	7.463	97.8	89.7	1.3
	2–0.5	6.54	9.110	97.6	78.6	1.0
	0.5–0.05	6.60	8.060	97.8	69.1	0.9
CD8	4–2	2.71	3.380	91.6	70.5	1.4
	2–0.5	4.69	5.955	94.6	71.8	1.0
	0.5–0.05	5.01	5.851	92.7	66.1	0.9
CD9	2–0.5	4.12	5.681	98.5	77.8	1.3
	0.5–0.05	3.36	4.197	94.0	70.6	1.1
CD15	< 2*	5.15	6.787	96.8	74.4	1.1
	2–0.5	5.33	7.206	96.9	76.3	1.0
CD17	2–0.5	3.32	4.717	95.1	80.1	1.1
PTO. 9	4–2	1.75	2.786	96.3	89.5	1.8
	2–0.5	3.99	5.061	93.2	71.7	1.2
	0.5–0.05	5.86	6.043	97.5	58.5	0.9
PTO. 11	4–2	2.07	2.944	92.2	80.2	1.7
	2–0.5	3.39	4.265	88.4	71.1	1.2
	0.5–0.05	3.37	3.045	96.1	51.4	1.2
PTO. 14	4–2	1.69	2.594	93.6	86.4	2.3
	2–0.5	5.85	8.245	97.9	79.5	1.2
	0.5–0.05	4.13	4.864	98.8	66.7	1.0
PTO. 15	4–2	2.46	4.293	93.3	97.9	1.6
	2–0.5	4.45	6.645	96.9	84.1	1.1
	0.5–0.05	4.40	4.996	96.7	64.3	0.9
PTO. 16	4–2	2.26	3.366	98.1	83.9	1.7
	2–0.5	4.94	5.856	97.4	67.1	0.9
	0.5–0.05	4.16	2.853	97.1	39.1	0.8

* Total clay fraction < 2 µm

Table 4. Closure temperature (°C) calculated for different grain sizes of muscovite following the model of Dodson (1973) and the diffusion parameters of Harrison et al. (2009).

Grain size (µm)*	10°C·Ma ⁻¹ #	100°C·Ma ⁻¹
2	317	343
1	303	327
0.5	289	312
0.1	260	280

* crystal radius; # Rate of cooling (in degrees Celsius per million years).

motions at the fault (e.g., Jaboyedoff and Cosca, 1999; Tagami, 2012).

Moreover, the age of whole < 2 µm fractions (Table 3) is very similar to the age of the coarse (2–0.5 µm) fraction, indicating that this size fraction is the most important volumetrically in every sample. This fact is seldom discussed in the literature, but it is usual to find, during the grain size separation of clays, that the percentage of samples diminishes largely with the grain size. The finest illite (<0.05 µm) is present in very small amounts, and in many cases is even impossible to extract.

Using the data from Figure 9 we interpret that only the very coarse illite fractions (2–4 µm) from the host rock (2M1 polytype) can be a mixture of neoformed 2M1 illite and minor proportions of detrital mica age. The deformation associated with the first tectonic episode (D1) involves the development of a slaty cleavage in the zone close to the fault, and KI values of illite-mica correspond to the limit from the high anchizone to epizone just below the ductile-brittle transition (Haines and van der Pluijm, 2008). We infer that the ages (80–75 Ma) obtained from these coarse fractions (2–0.5 µm) at the fault zone document this first and most important fault movement. The ages for the finest fractions (50–40 Ma) are interpreted as the last tectonic event related to the orogenic wedge in this zone, with concomitant diagenesis.

The ages of the medium illite fractions (0.5–0.05 µm) at the fault zone are more difficult to interpret. The reactivation of the El Doctor shear zone produced folding and crenulation of the previous foliation (D2), successively cut by meter-scale extensional shear bends (D3). During late low-temperature reactivation of the fault, old authigenic illite-mica ages were not reset, and a new batch of authigenic illite was formed through nucleation and crystal growth processes. Figure 10 presents a synthetic interpretation of illite growth in the El Doctor

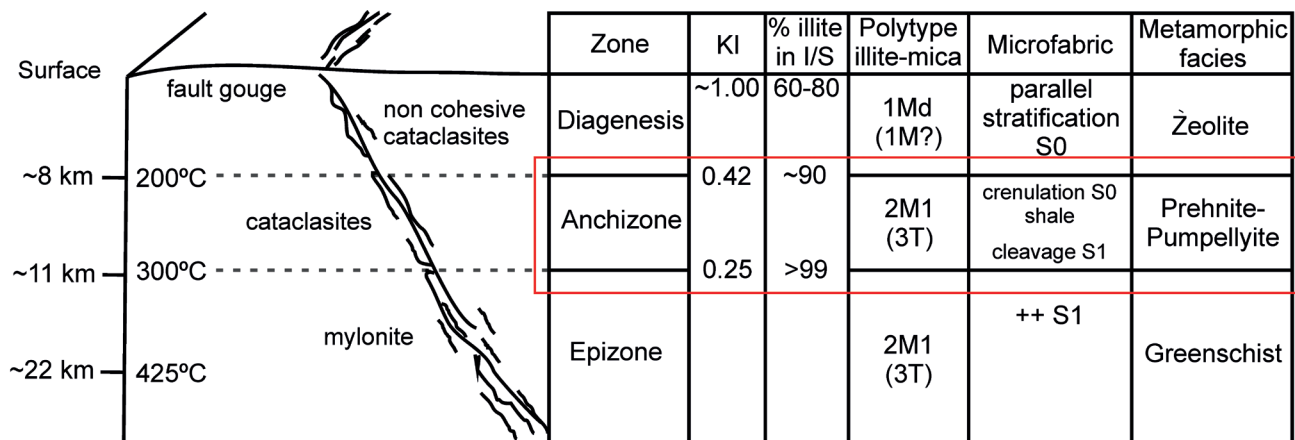


Figure 9. Synoptic model of a suture zone from Scholz (1988) and Abad (2006), showing the schematic section across the fault zone, along with illite parameters compared with temperature or depth. The red box shows the deformation conditions of the El Doctor Fault. KI: Kübler Index, % illite in I/S: percentage of illite in illite-smectite mixed-layered clays.

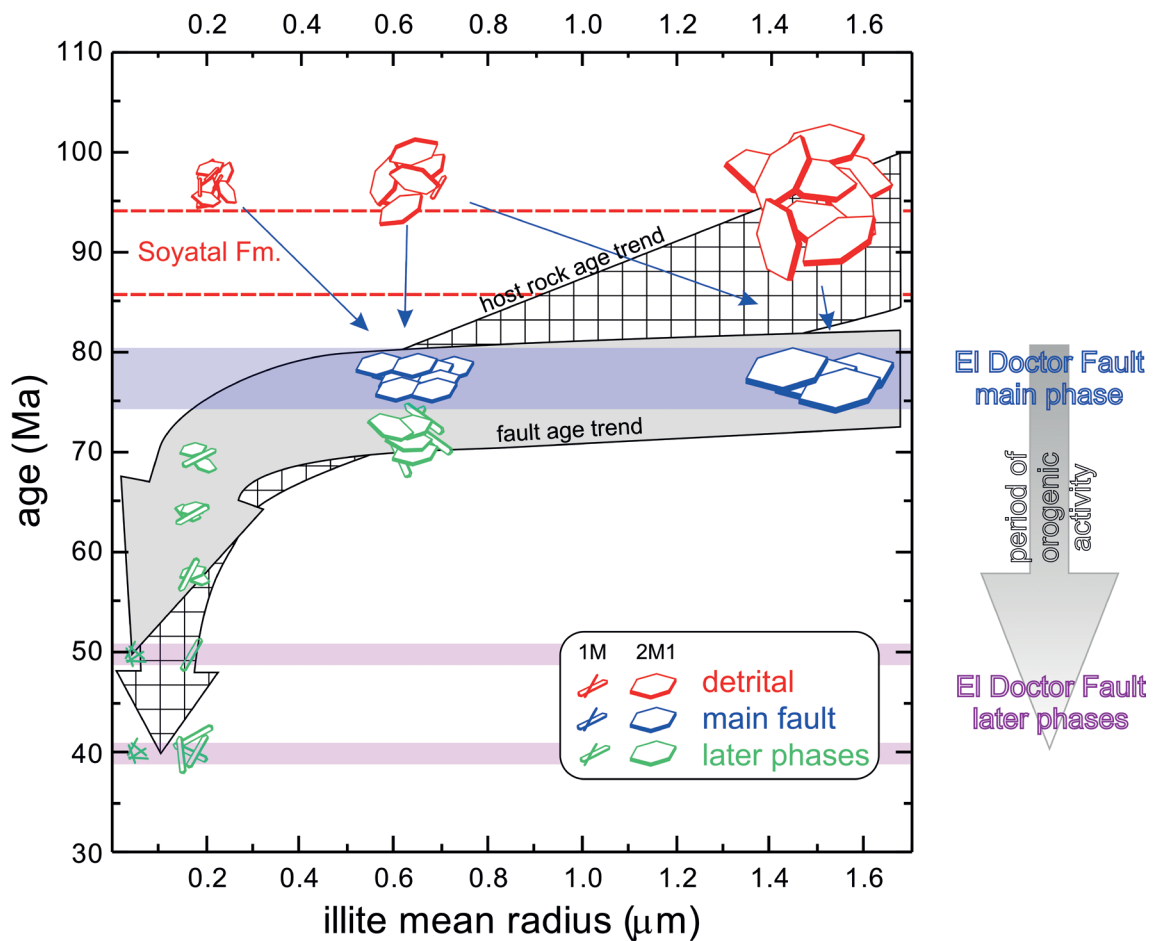


Figure 10. Conceptual model for the interpretation of K-Ar age versus grain size patterns obtained in this work. Two trends are observed: (a) ages from the fault zone, and (b) ages from the host rock (Soyatal Formation). The coarse fractions from the fault zone date the earliest and most important tectonic event at the El Doctor fault (blue color). The finest size fraction from the fault zone dates the timing of the last fault reactivation (green color). The host rock age trend presents an inherited (detrital, red color) age for the very coarse fractions which intersect the fault age trend at the coarse fractions and decrease to lower ages in the finest fractions. This trend is indicative of a detrital component which is partially reset during the formation of the tectonic wedge and contains very small neofomed illites due to the last tectonic movements and diagenesis.

fault and the host rock (Soyatal Formation) at different distances from the fault (Figure 1). It is noteworthy that the whole tectonic pile is deformed, with the consequence of illites everywhere having a range of ages. The oldest ages are found in the coarse mica from the host rock, due to the lack of the pervasive recrystallization found in the fault. The youngest ages are found in the finest fractions, also in the host rock, probably due to the simultaneous diagenesis. The latter has been stronger in the host rock, because it was tectonically located *below* the El Doctor fault in the sampling zone.

The tectonic wedge model

In our opinion the general interpretation clue is the tectonic model of the orogenic wedge. Analog and numerical models (e.g., Stockmal *et al.*, 2007; Buitier, 2012; Jamieson and Beaumont, 2013) show that during wedge progression, creation and displacement of thrusts begins near the region of initial stress (*i.e.*, the region where the 'bulldozer' pushes the wedge) and translates to the foreland. The progression is visible by the propagation of deformation in that direction. The oldest deformation will be located near the 'bulldozer', and the youngest deformation will be on the opposite side. In the case of the MFTB, the oldest deformation must be in the West and the youngest deformation is in the East, as discussed in a previous section. This age progression has been found

by indirect dating in a W-E section across Central Mexico by Cuéllar-Cárdenas *et al.* (2012). Nevertheless, all analog and numerical models (*op. cit.*) show that during the progression of the wedge, the oldest part ('fossilized' following the simplistic models) is in fact reworked several times taking advantage of the weaker zones, *i.e.*, previous faults and thrusts. This translates to the classical observation of faults which show various episodes of movement.

Dating of clays associated with such faults cannot give a single age, unless the fault has remained at high temperature and pressure (probably no longer a fault but a shear zone). In the normal case of anchizone-low epizone faults and thrusts, clays must provide a range of ages, indicating episodes of clay growth related to fault movement and associated fluid circulation.

The Laramide orogeny

The Laramide orogeny is the credited cause for the development of the main Late Mesozoic-Early Cenozoic structures of Central Mexico (e.g. Cuéllar-Cárdenas *et al.*, 2012), including the El Doctor fault. We do not wish to discuss this attribute, but we do wish to mention four points. Firstly, the Laramide orogeny is not much older than ~75 Ma (e.g., Bird, 2002), as defined in the original outcrops from the USA. Secondly, older deformation starting at ~120 Ma is defined as the

Sevier orogeny (e.g., Heller and Paola, 1989). Thirdly, it is not clear that both orogenies, defined in the USA, can be extrapolated to Mexico in both cause and timing. Finally, de Cserna (1960) and Guzmán and de Cserna (1963) defined the Hidalgoan orogeny in Eastern Mexico as being simultaneous with the Sevier orogeny and spanning as late as ~52 Ma overlapping with the Laramide orogeny.

Following this unclear scenario, the best we can do is to name the Mexican orogeny as Laramide *sensu lato*, to be consistent with the many publications about Mexican tectonics, and to make clear that any attribution to one or another orogenic name defined in the USA is, at least, uncertain. Our interpretation suggests that most of the history of the MFTB is recorded in a single regional scale thrust which undergoes repeated reactivations during development of the orogen.

CONCLUSIONS

The El Doctor fault is an important structure located in the MFTB that superposes the slight deformed rocks of the El Doctor Formation (Albian-Cenomanian period) over tubiditic synsedimentary rocks from the Soyatal Formation (Turonian-Coniacian period). The fault core displays a high anchizone-low epizone texture and mineralogy.

The occurrence of neoformed illite-mica layers oriented along the fabric of the fault core and suggests a process of dissolution and recrystallization of this mineral. Based on available data and closure temperature calculations we can infer that its age records the time elapsed since authigenic mineral growth within the fault zone, because during recrystallization radiogenic argon was lost from the <2 µm crystals.

Different faulting episodes were accommodated by the El Doctor fault and the K-Ar ages define a time range during which the fault was active. K-Ar data from illite-mica support a model in which the El Doctor thrust formation occurred at 80–75 Ma. This age is obtained from the coarse clay fractions (2–0.5 µm), which are younger than the age of sedimentation of the Soyatal Formation. The youngest ages of 50 and 40 Ma indicate 1M illite formation by later events related to fault movement plus diagenesis.

The significance of intermediate ages which decrease with grain size cannot be deciphered with the available data, but can be interpreted considering a mixing between an authigenic illite-mica generation formed during the main fault phase and a younger authigenic low-temperature illite. The correlation of fault movements to these ages cannot be ruled out.

The age of the El Doctor fault is in concordance with the term Laramide age *sensu lato* defined above, i.e. a deformation active between the Cenomanian and Eocene periods (e.g., Schmidt and Perry, 1988; Gray *et al.*, 2001). The K-Ar ages of illite suggest that, in this part of the Mexican Fold and Thrust Belt, deformation remains active during the whole development of the orogenic wedge.

ACKNOWLEDGEMENTS

Support for this work was provided by CONACYT Ciencia Básica grant number 167514 to Teresa Pi Puig and a CONACYT scholarship to Diana Garduño. We acknowledge Margarita Reyes Salas and Sonia Ángeles García at the Instituto de Geología of UNAM and Eduardo Palacios from the Instituto Mexicano del Petróleo for the use of the SEM facilities, and Patricia Girón for K determinations. We are grateful to Alexander Iriondo, Angel Nieto Samaniego and Peter Schaaf who reviewed the manuscript and made useful suggestions to improve it.

REFERENCES

- Abad I., 2006, Physical meaning and applications of the illite Kübler index: measuring reaction progress in low-grade metamorphism: *Seminarios de la Sociedad Española de Mineralogía*, 3-53.
- Bailey, S.W., Hurley, P.M., Fairbairn, H.W., Pinson, W.H.Jr., 1962, K-Ar dating of sedimentary illite polytypes: *Bulletin of the Geological Society of America*, 73, 1167.
- Bird, P., 2002, Stress direction history of the western United States and Mexico since 85 Ma: *Tectonics*, 21, 10.1029/2001TC001319, 12 pp.
- Brindley G.W., Brown G. (editors) 1980, *Crystal structures of clay minerals and their X-ray identification*: 41 Queen's Gate, London SW7 5hr, Mineralogical Society, 495 pp.
- Buiter, S.J.H., 2012, A review of brittle compressional wedge models: *Tectonophysics*, 530-531, 1-17.
- Clauer, N., 2013, The K-Ar and ⁴⁰Ar/³⁹Ar methods revisited for dating and tracing low-temperature K-bearing clay minerals: *Chemical Geology*, 354, 163-185.
- Clauer, N., Chaudhuri, S., 1995, *Clays in Crustal Environments*, in *Isotope Dating and Tracing*: Berlin, Springer-Verlag, 359 p.
- Clauer, N., Srodoń, J., Francu, J., Sucha, V., 1997, K-Ar dating of illite fundamental particles separated from illite/smectite: *Clay Minerals*, 32, 181-196.
- Cuéllar-Cárdenas, M.A., Nieto-Samaniego, A.F., Levrèse, G., Alaniz-Álvarez S.A., Solari, L., Ortega-Obregón, C., López-Martínez, M., 2012, Límites temporales de la deformación por acortamiento Laramide en el centro de México: *Revista Mexicana de Ciencias Geológicas*, 29(1), 179-203.
- Dahlen, F. A., 1990, Critical taper model of fold and thrust belts and accretionary wedges: *Annual Reviews Earth Planetary Sciences*, 18, 55-99.
- Dahlen, F. A., Suppe, J. Davis, D., 1984, *Mechanics of Fold-and-Thrust Belts and Accretionary Wedges: Cohesive Coulomb Theory*: *Journal of Geophysical Research*, 89-B12, 10087-10101.
- de Cserna Z., 1960, Orogenesis in time and space in Mexico: *Geologische Rundschau* 50(1), 595-605.
- Dodson, M.H., 1973, Closure temperature in cooling geochronological and petrological systems: *Contributions to Mineralogy and Petrology*, 40, 259-274.
- Dong, H., Hall, C. M., Peacor, D., Halliday, A. N., 1995, Mechanisms of argon retention in clays revealed by laser ⁴⁰Ar-³⁹Ar dating: *Science* 267, 355-359.
- Drits V.A., Besson G., Muller F., 1995, An improved model for structural transformations of heat-treated aluminous dioctahedral 2:1 layer silicates: *Clays and Clay Minerals*, 43, 718-31.
- Drits V.A., Lindgreen H., Salyn A.L., Ylagan R.F., McCarty D.K., 1998, Semiquantitative determination of trans-vacant and cis-vacant 2:1 layers in illites and illite-smectites by thermal analysis and X-ray diffraction: *The American Mineralogist*, 83, 1188-1198.
- Duvall, A.R., Clark, M.K., van der Pluijm, A., Li, C., 2011, Direct dating of Eocene reverse faulting in northeastern Tibet using Ar-dating of fault clays and low-temperature thermochronometry: *Earth and Planetary Science Letters*, 304 (3-4), 520-526.
- Eberl, D.D., Drits, V.A., Srodoń, J., 1999, Deducing growth mechanisms for minerals from the shapes of crystal size distributions: *American Journal of Science*, 298, 499-533.
- Fitz-Díaz, E., 2010, *Progressive deformation, fluid flow and water-rock interaction in the Mexican Fold-Thrust Belt*, Central Mexico: USA, University of Minnesota, PhD Thesis, 152 pp.
- Fitz-Díaz, E., Hudleston, P. Tolson, G., 2011, Comparison of tectonic styles in the Mexican and Canadian Rocky Mountain Fold-Thrust Belt, in Poblet J., Lisle R. (eds.), *Kinematics and Tectonic Styles of Fold-Thrust Belt*: Geological Society of London, Special Publication, 349, 149-167.
- Fitz-Díaz, E., Tolson, G., Hudleston, P., Bolaños-Rodríguez, D., Ortega-Flores, B., Vázquez-Serrano, A., 2012, The role of folding in the development of the Mexican Fold-Thrust Belt: *Geosphere*, doi:10.1130/GES00759.1.
- Fitz-Díaz, E., van der Pluijm, B., Hudleston, P., Tolson, G., 2014, Progressive, episodic deformation in the Mexican Fold-Thrust Belt (Central Mexico): evidence from isotopic dating of folds and faults: *International Geology Review* 56(6), 734-755.
- Grathoff, G. H., Moore, D. M., 1996, Illite polytype quantification using WILDFIRE calculated X-ray diffraction patterns: *Clays and Clay Minerals*, 44, 835-842.

- Gray, G.G., Pottorf, R.J., Yurewicz, D.A., Mahon, K.I., Pevear, D.R., Chuchla, R.J., 2001, Thermal and chronological record of syn-to post-Laramide burial and exhumation, Sierra Madre Oriental, Mexico: American Association of Petroleum Geologists Memoir, 75, 159-181.
- Guzmán, J.E., de Cserna, Z., 1963, Tectonic history of Mexico, in Backbone of the Americas-Tectonic History, a Symposium: American Association of Petroleum Geologists Memoir, 2, 113-129.
- Haines, S., van der Pluijm, B., 2008, Clay quantification and Ar-Ar dating of synthetic and natural gouge: Journal Structure Geology, 30, 525-538.
- Hamilton, P.J., Giles, M.R. and Ainsworth, P., 1992, K-Ar dating of illites in Brent Group reservoirs: a regional perspective. in Morton, A.C. *et al.*, (eds.), Geology of the Brent Group, Special Publication: London, Geological Society of London, 61, 377-400.
- Harrison, T.M., Celerier, J., Aikman, A.B., Hermann, J., Heizler, M.T., 2009, Diffusion of ^{40}Ar in muscovite: Geochimica et Cosmochimica Acta, 73, 1039-1051.
- Heller, P., Paola, C., 1989, Then paradox of Lower Cretaceous gravels and the initiation of thrusting in the Sevier orogenic belt, United States western interior: Geological Society of America Bulletin, 101, 864-875.
- Hernández-Jáuregui, R., 1997, Sedimentación sintectónica de la Formación Soyatal (Turoniano medio-Campaniano) y modelado cinemático progresivo de la cuenca de flexura de Maconí, Querétaro: México, ESIA, Instituto Politécnico Nacional, Tesis de Maestría, 120 pp.
- Hunziker, J.C., Frey, M., Clauer, N., Dallmeyer, R., Friedrichsen, H., Flehmig, W., Hochstrasser, K., Roggwiler, P., Schwander, H., 1986, The evolution of illite to muscovite: mineralogical and isotopic data from the Glarus Alps, Switzerland: Contributions to Mineralogy and Petrology, 92, 157-180.
- Hurley, P.M., Hart, S.R., Pinson, W.H., Fairbairn, H.W. 1959, Authigenic versus detrital illite in sediments (abstract): Bulletin of the Geological Society of America, 70, 1622.
- Inoue, A., Velde, B., Meunier, A. Touchard, G., 1988, Mechanism of illite formation during smectite to illite conversion in a hydrothermal system: The American Mineralogist, 73, 1325-1334.
- International Commission on Stratigraphy, 2014, International Chronostratigraphic Chart v2014/10. <http://www.stratigraphy.org/>
- Jaboyedoff, M., Cosca, M.A., 1999, Dating incipient metamorphism using $^{40}\text{Ar}/^{39}\text{Ar}$ geochronology and XRD modeling: A case study from the Swiss Alps: Contributions to Mineralogy and Petrology, 135(2-3), 93-113.
- Jackson, M.L., 1985, Soil Chemical Analysis-Advanced Course. A Manual of Methods Useful for Instruction and Research in Soil Chemistry, Physical Chemistry of Soils, Soil Fertility, and Soil Genesis. Second Edition, Revised from original edition of 1956, Published by the Author.
- Jamieson, R.A., Beaumont, C., 2013, On the origin of orogens: Geological Society of America Bulletin, 125, 1671-1702.
- Kisch, H.J., 1990, Calibration of the anchizone: a critical comparison of illite "crystallinity" scales used for definition: Journal of Metamorphic Geology, 8, 31-46.
- Kisch, H.J., 1991, Illite crystallinity: recommendations on sample preparation, X-ray diffraction settings, and interlaboratory samples: Journal of Metamorphic Geology, 9, 665-670.
- Kübler, B., 1967, La cristallinité de l'illite et des zones tout à fait supérieures du métamorphisme, in Étages tectoniques, Colloque de Neuchâtel, 1966: Switzerland, A la Baconnière Neuchâtel, 105-121.
- Kübler, B., 1968, Evaluation quantitative du métamorphisme par la cristallinité de l'illite: Bulletin du Centre de Recherches de Pau-SNPA, 2, 385-397.
- Kübler, B., Jaboyedoff, M., 2000, Illite crystallinity: Comptes Rendus de l'Académie des Sciences de Paris, Sciences de la Terre et des Planètes, 331, 75-90.
- Lanson, B., 1997, Decomposition of experimental X-ray diffraction patterns (profile fitting): A convenient way to study clay minerals: Clays and Clay Minerals, 45, 132-146.
- Lanson, B., Besson, G., 1992, Characterization of the smectite-to-illite transformation: Decomposition of X-ray patterns: Clays and Clay Minerals, 40, 40-52.
- Liewig, N., Clauer, N., Sommer, F., 1987, Rb-Sr and K-Ar dating of clay diagenesis in Jurassic sandstone oil reservoirs, North Sea: American Association of Petroleum Geology Bulletin, 71, 1467-1474.
- López-Ramos, E., 1983, Estratigrafía Cretácica y tectónica de una porción del centro y noreste de México. Cretaceous stratigraphy and tectonics of a portion of the central and northeast of Mexico: Boletín de la Sociedad Geológica Mexicana, 44(1), 21-31.
- Lyons, J.B., Snellenburg, J., 1971, Dating faults: Geological Society of America Bulletin, 82, 1749-1752.
- Martini, M., Fitz, E., Solari, L., Camprubi, A., Hudleston, P.J., Lawton, T.F., Tolson, G., Centeno-García, E., 2012, The Late Cretaceous fold-thrust belt in the Peña de Bernal-Tamazunchale area and its possible relationship to the accretion of the Guerrero Terrane, in Aranda-Gómez, J.J., Tolson, G., Molina-Garza, R.S. (eds.), The Southern Cordillera and Beyond: Geological Society of America Field Guide 25, 19-38
- Maxwell, D.T., Hower, J., 1967, High-grade diagenesis and low-grade metamorphism of illite in the Precambrian Belt Series: The American Mineralogist, 52, 843-857.
- Merriman, R.J., Peacor, D.R., 1999, Very low grade metapelites: mineralogy, microfabrics and measuring reaction progress, in Frey, M., Robinson, D. (eds.), Low-Grade Metamorphism: Oxford, Blackwell, Science, 10-60.
- Meunier, A., Velde, B.D., 2004, Illite: Origins, Evolution and Metamorphism: Berlin, Heidelberg, Springer-Verlag, 286 pp, ISBN 978 3 540 20486 2
- Meunier, A., Velde, B., Zalba, P., 2004, Illite K-Ar dating and crystal growth processes in diagenetic environments: a critical review: Terra Nova, 16, 296-304.
- Middleton, A.W., Uysal, I.T., Bryan, S.E., Hall, C. M., Golding, S.D., 2014, Integrating ^{40}Ar - ^{39}Ar , ^{87}Rb - ^{87}Sr and ^{147}Sm - ^{143}Nd geochronology of authigenic illite to evaluate tectonic reactivation in an intraplate setting, central Australia: Geochimica et Cosmochimica Acta, 134, 155-174.
- Moore, D.M., Reynolds, R.C.Jr., 1997, X-ray diffraction and the identification analysis of clay minerals: Oxford and New York, Oxford University Press, 352 pp.
- Omaña Pulido, R.M. de L., 2012, Biostratigrafía, Paleoecología y Paleobiogeografía del Cretácico Superior con base en foraminíferos de la parte occidental de la Plataforma Valles-San Luis Potosí, México: México, Universidad Nacional Autónoma de México, PhD Thesis, 198 pp.
- Ortega-Flores, B., 2010, Deformación por acortamiento en la Plataforma Valles-San Luis Potosí y en la Cuenca Tampico-Misantla; porción externa del Cinturón de Pliegues y Cabalgaduras Mexicanas: México, Programa de Posgrado en Ciencias de la Tierra, Universidad Nacional Autónoma de México, M.Sc. Thesis, 100 pp.
- Passchier, C.W., Trouw, R.A.J., 1998, Microtectonics: New York, Springer, 289 pp.
- Pevear, D.R., 1999, Illite and hydrocarbon exploration: Proceedings of the National Academy of Sciences, 96, 3440-3446.
- Reynolds, R.C., Jr., 1992, X-ray diffraction studies of illite/smectite from rocks, <1 μm randomly oriented powders, and <1 μm oriented powder aggregates; the absence of laboratory-induced artifacts: Clays and Clay Minerals, 40, 387-396.
- Reynolds, R.C.Jr., 1993, WILDFIRE ©: A Computer Program for the Calculation of Three-Dimensional Powder X-ray Diffraction Patterns for Mica Polytypes and Their Disordered Variations: Hannover, New Hampshire, 76 pp.
- Reynolds, R.C., Jr., 1994, Interstratified clay systems: calculation of the total one-dimensional diffraction function: The American Mineralogist, 52, 661-672.
- Schleicher, A., Warr, L., Kober, B., Laverret, E., Clauer, N., 2006, Episodic mineralization of hydrothermal illite in the Soultz-sous-Forêts granite, Upper Rhine Graben, France: Contributions to Mineralogy and Petrology, 152(3), 349-364.
- Schmidt, C.J., Perry, W.J.Jr., 1988, Interaction of the Rocky Mountain foreland and the Cordilleran thrust belt: Geological Society of America Memoir, 171, 582.
- Scholz, C.H., 1988, The brittle-plastic transition and the depth of seismic faulting: Geologische Rundschau, 77, 319-328
- Siebel, W., Hann, H.P., Danišik, M., Shang, C.K., Berthold, Ch., Rohrmüller, J., Wemmer, K., Evans, N.J., 2010, Age constraints on faulting and fault reactivation: a multi-chronological approach: International Journal of Earth Sciences, 99(6), 1187-1197.
- Solé, J., 2009, Determination of K-Ar ages in milligram samples using an infrared laser for argon extraction: Rapid Communications in Mass Spectrometry, 33, 3579-3590.
- Solé, J., Enrique, P., 2001, X-ray fluorescence analysis for the determination of potassium in small quantities of silicate minerals for K-Ar dating: Analytica

- Chimica Acta, 440, 199–205.
- Solum, J.G., van der Pluijm, B. A., Peacor, D.R., 2005, Neocrystallization, fabrics and age of clay minerals from an exposure of the Moab Fault: *Journal of Structural Geology*, 27, 1563–1576.
- Środoń, J., 1984, X-ray powder diffraction identification of illitic materials: *Clays and Clay Minerals*, 32, 337–349.
- Środoń, J., 2002, Quantitative mineralogy of sedimentary rocks with emphasis on clays and with applications to K-Ar dating: *Mineralogy Magazine*, 66, 677–687.
- Środoń, J., Eberl D.D., 1984, Illite in Bailey, S.W. (ed.), *Micas: Reviews in Mineralogy*, Mineralogical Society of America, 13, 495–544.
- Środoń, J., Drits, V.A., McCarty, D.K., Hsieh, J.C.C., Eberl, D.D., 2001, Quantitative X-Ray Diffraction analysis of clay-bearing rocks from random preparations: *Clays and Clay Minerals*, 49(6), 514–528.
- Stockmal, G.S., Beaumont, C., Nguyen, M., Lee, B., 2007, Mechanics of thin-skinned fold-and-thrust belts: Insights from numerical models: *Geological Society of America Special Papers*, 433, 63–98.
- Surace, I.R., Clauer, N., Thélin, P., Pfeifer, H.R., 2011, Structural analysis, clay mineralogy and K-Ar dating of fault gouges from Centovalli Line (Central Alps) for reconstruction of their recent activity: *Tectonophysics*, 510, 80–93.
- Suter, M., 1980, Tectonics of the external part of the Sierra Madre Oriental foreland thrust and fold belt Between Xilitla and the Moctezuma River (Hidalgo and San Luis Potosí states): *UNAM, Revista del Instituto de Geología*, 4, 19–31.
- Suter, M., 1984, Cordilleran deformation along the eastern edge of the Valles-San Luis Potosí carbonate platform, Sierra Madre Oriental thrust and fold belt, east-central Mexico: *Geological Society of America Bulletin*, 95, 1387–1397.
- Suter, M., 1987, Structural traverse across the Sierra Madre Oriental fold-thrust belt in east-central Mexico: *Geological Society of America Bulletin*, 98, 249–264.
- Tagami, T., 2012, Thermochronological investigation of fault zones: *Tectonophysics*, 538–540, 67–85.
- Torgersen, E., Viola, G., Zwingmann, H., Harris, C., 2015, Structural and temporal evolution of a reactivated brittle-ductile fault – Part II: Timing of fault initiation and reactivation by K-Ar dating of synkinematic illite/muscovite: *Earth and Planetary Science Letters*, 410, 212–224.
- van der Pluijm, B.A., Hall, C.M., Vrolijk, P.J., Pevear, D.R., Covey, M.C., 2001, The dating of shallow faults in the Earth's crust: *Nature*, 412, 172–175.
- van der Pluijm, B. A. Vrolijk, P. J. Pevear, D. R. Hall, C. M., Solum, J., 2006, Fault dating in the Canadian Rocky Mountains; evidence for Late Cretaceous and early Eocene orogenic pulses: *Geology*, 34(10), 837–840.
- Verdel, Ch., Niemi, N., van der Pluijm, B. A., 2011a, Variations in the Illite to Muscovite Transition Related to Metamorphic Conditions and Detrital Muscovite Content: Insight from the Paleozoic Passive Margin of the Southwestern United States: *The Journal of Geology*, 119, 419–437.
- Verdel, C., Niemi, N., van der Pluijm, B. A., 2011b, Thermochronology of the Salt Spring fault: constraints on the evolution of the South Virgin–White Hills detachment system, Nevada and Arizona, USA: *Geosphere*, 7, 774–784.
- Viola, G., Zwingmann, H., Mattila, J., Käpyaho A., 2013, K-Ar illite age constraints on the Proterozoic formation and reactivation history of a brittle fault in Fennoscandia: *Terra Nova*, 25(3), 236–244.
- Vrolijk, P., van der Pluijm, B. A., 1999, Clay gouge; questions in structural geology; 20th anniversary special issue: *Journal of Structural Geology*, 21(8–9), 1039–1048.
- Wojdyr, M., 2010, Fityk: a general-purpose peak fitting program: *Journal of Applied Crystallography*, 43, 1126–1128.
- Ylagan, R.F., Pevear, D.R., Vrolijk, P.J., 2000, Discussion of “Extracting K-Ar Ages From Shales: A Theoretical Test”: *Clay Minerals*, 35, 599–604.
- Ylagan, R., Kim, C., Pevear, D., Vrolijk, P., 2002, Illite polytype quantification for accurate K-Ar determination: *The American Mineralogist*, 87, 1536–1545.
- Zwingmann, H., Mancktelow, N.S., 2004, Timing of Alpine fault gouges: *Earth and Planetary Science Letters*, 223, 415–425.
- Zwingmann, H., Mancktelow, N., Antognini, M., Lucchini, R., 2010a, Dating of shallow faults – new constraints from the AlpTransit tunnel site (Switzerland): *Geology*, 38, 487–490.
- Zwingmann, H., Yamada, K., Tagami, T., 2010b, Timing of brittle faulting within the Nojima fault zone, Japan: *Chemical Geology*, 275, 176–185.
- Zwingmann, H., Han, R. Ree, J.H., 2011, Cretaceous reactivation of the Deokpori Thrust, Taebaeksan Basin, South Korea, constrained by K-Ar dating of clayey fault gouge: *Tectonics*, 30, TC5015.

Manuscript received: November 11, 2013

Corrected manuscript received: March 3, 2015

Manuscript accepted: April 9, 2015